A Search for Fast Pulsars in Globular Clusters

by

Steve Bégin

B.Sc., Université Laval, 2003

A THESIS SUBMITTED IN PARTIAL FULFILMENT OF
THE REQUIREMENTS FOR THE DEGREE OF

Master of Science

in

The Faculty of Graduate Studies

(Physics)

The University Of British Columbia

October 2006

Abstract

Millisecond pulsars (MSP) are old neutron stars that have been spun up to high spin frequencies (as fast as 716 Hz) through the accretion of matter from a companion star. The extreme stellar densities in the core of globular clusters creates numerous accreting neutron star systems through exchange interactions; this leads to the formation of MSPs in larger numbers than in the galactic disk. Over the course of this project, we have collected over 17 TB of data on the 3 globular clusters M28, NGC6440 and NGC6441 plus 2 observations on NGC6522 and NGC6624 as part of the recently begun S-band survey using the Green Bank telescope. I have analyzed and conducted acceleration searches on 70% of the data and discovered 7 of the 23 new millisecond pulsars reported in this work. One year of timing observations of the pulsars in M28 and NGC6440 has led to the phase connected solution for 12 of the 15 new pulsars in those two clusters, 7 of which are in binaries. We have measured the rate of advance of periastron for two highly eccentric binaries and assuming this is purely due to general relativity, this leads to total system masses of $(1.616 \pm 0.014)M_{\odot}$ and $(2.2 \pm 0.8)M_{\odot}$ for M28C and NGC6440B respectively. The small mass function combined with this information imply that the most likely neutron star mass of NGC6440B is either very large or else there could be significant contribution to the advance of periastron from a nonzero quadrupole moment due to tidal interaction with the companion. Measurements of the period derivatives for many of the pulsars show that they are dominated by the dynamical effect of the gravitational field of the clusters. Finally, we have discovered the potential presence of a Mars-mass planet orbiting the pulsar NGC6440C with a period of $\sim$21 days. A dedicated timing campaign will be necessary to confirm the presence of such an object.

Steve Bégin.

sbegin@phas.ubc.ca

Contents

List of Tables

List of Figures

Acknowledgements

I would like to thank my supervisor, Dr. Ingrid Stairs, for sharing with me part of her (seemingly) boundless knowledge of pulsar astronomy but also for the countless hours spent in my company so that I could learn the intricacies of pulsar timing. Without her precious help, this thesis would not have been possible. I want to thank Scott Ransom for guiding me on my quest to find new pulsars as well as for a good day of climbing in Virginia. I want to thank my collaborators Paulo Freire and Jason Hessels for their helpful advice and contagious enthusiasm. I want to thank my pulsar workmates: Rob "The supreme being of all Universes", Joeri "vanPython" and Laura "Krazian" for the exciting discussions about various aspect of our work. I appreciated every coffee break in your company. Special thanks to my Mom who was visiting during the busiest time of this whole project. Your presence was comforting, and your cooking, simply the best. Finally, I would like to give a shout to Jacqui, my everyday source of inspiration.

Chapter 1

Introduction

1.1 Brief History of Radio Pulsars

The discovery of the neutron (Chadwick, 1932) quickly led to the concept of the neutron star (Baade and Zwicky, 1934). Together they proposed the concept and predicted their fundamental properties. In 1938, neutron star sizes and densities were estimated (Landau, 1938) and one year later, their structure derived (Oppenheimer and Volkoff, 1939). It was quickly realized that they would be too small to be observed directly. Nevertheless, pulsars were discovered in 1967 by Jocelyn Bell, working under the supervision of her thesis adviser, Antony Hewish. Using a new telescope near Cambridge specifically designed to study the rapid scintillation of radio signals from quasars as they propagated through the solar wind, Bell noticed a signal that had the form of a series of short radio pulses, repeated every 1.337 seconds. A distance estimate of 65 parsecs was obtained for the first object, from measurement of the dispersion of the signal in the ionized interstellar medium, placing the source far beyond the solar system (Hewish et al., 1968).

1.2 Normal, Binary and Millisecond Pulsars

1.2.1 Pulsar properties

Pulsars are rapidly spinning neutron stars with incredibly strong magnetic fields that produce beams of electromagnetic radiation that may sweep past the Earth with each rotation of the star. The resulting pulses are observed primarily at radio wavelengths. Neutron stars are one of the 2 possible outcomes (the other being black holes) of the death of a massive star in a supernova. From direct and accurate measurements made from timing observation of pulsars, the masses of neutron star are typically between 1.3 and 2.0 $M_{\odot}$ (Stairs, 2004) with various models predicting radii on the order of 10 km (Lattimer and Prakash, 2001). Using canonical values for the mass and the radius (M = 1.4 $M_{\odot}$, R = 10 km), the mass density of neutron stars can be shown to be comparable to that of an atomic nucleus, with an average value $\rho_{\mathrm{avr}} = 6.7 \times 10^{14}$ g/cm^3 reaching up to 10$\times$ the nuclear density in the center. The value for the moment of inertia, supposing a sphere of uniform density, is I = 10^{45} g cm^2. Most likely, this value is highly approximate but nevertheless useful for order-of-magnitude calculations. Neutron stars also have extremely high surface gravity, $\approx 2 \times 10^{11}$ times stronger than that of Earth, translating to an escape velocity of the order of 150000 km s^{-1}. See, for example, Shapiro and Teukolsky (1983) for a description of neutron stars and Lyne and Smith (1998) for general information on pulsars.

The standard interpretation of the pulsating radio signals is that they are produced via the lighthouse effect in which the emission beam, locked to the surface of a rotating neutron star, sweeps past our line of sight every rotation. Although the process by which the radio pulsation is emitted is not understood at the moment, it is likely to be the result of the acceleration of charged particles along the magnetic field lines of the pulsar (Goldreich and Julian, 1969). Despite our lack of understanding of the emission process, their incredible stability as rotators, studied from pulsar timing, provides us with very useful information.

1.2.2 Spin evolution

Except for some pulsars in globular clusters (as we will see in chapter 4), the spin periods of pulsars are observed to increased with time. The intrinsic rate of change of the spin period is an important characteristic of a pulsar and can be obtained from least-squares fitting of the observed pulse arrival times (more on that in chapter 3). This loss of rotational kinetic energy is usually attributed to the dipole radiation from the strong magnetic field of neutron stars but is also in part due to the outflow of particles (e.g. Kramer et al., 2006). The evolution of the rotation frequency can be expressed as a power law

$$\dot{\nu} = -K\nu^n \tag{1.1}$$

where n is known as the *braking index*. For pure dipole radiation, the braking index would be $n = 3$, but observations show that this is rarely the case with values ranging from $n = 1.4$ to $n = 2.9$ (Kaspi and Helfand, 2002).

Surface magnetic field estimate If we make the assumption that the pulsar is a perfect magnetic dipole, we can get an estimate of its magnetic field strength from the pulsar's period and period derivative. The expression for the pulsar surface field strength, assuming that the spin-down process is dominated by the dipole braking (e.g., Lorimer and Kramer, 2005)

$$B_s = \sqrt{\frac{3c^3}{8\pi^2} \frac{I}{R^6 \sin^2 \alpha} P\dot{P}} \tag{1.2}$$

where α is the angle between the spin axis and the magnetic moment. Assuming $\alpha = 90°$, we find the *characteristic magnetic field* equation

$$B_s = 3.2 \times 10^{19} \sqrt{P\dot{P}} \text{ G} \tag{1.3}$$

Because the values for the masses and radii of neutron stars are highly uncertain and α is usually unknown, this equation should be used only for order-of-magnitude estimates.

Pulsar age estimate We can also obtain an estimate of the age of the pulsar by integrating equation 1.1 expressed in terms of pulse period (Lorimer and Kramer, 2005). For a braking index $n \neq 1$, the age of the pulsar is

$$T = \frac{P}{(n-1)\dot{P}} \left[1 - \left(\frac{P_0}{P} \right)^{n-1} \right] \tag{1.4}$$

where P_0 is the pulsar spin period at birth. We can further simplify the expression by assuming that the spin down is due to dipole radiation (n=3) and that the pulsar's spin period at birth is much shorter than its current value ($P_0 \ll P$), leading to the *characteristic age* equation

$$\tau_c = \frac{P}{2\dot{P}} \simeq 15.8 \left(\frac{\dot{P}}{10^{-15}} \right)^{-1} \left(\frac{P}{s} \right) \text{ Myr} \tag{1.5}$$

Unfortunately, this is not a very accurate way to determine the age of any pulsar and, again, should be used for order of magnitude estimates only. For example, the radio pulsar J0205+6449 is probably associated with the supernova of AD 1181. The value calculated from eq. 1.5 yields $\tau_c = 5370$ yr (e.g. Camilo et al., 2002).

1.2.3 From Normal to Millisecond pulsars

The fastest rotating neutron star currently known is PSR J1748-2446ad spinning at an incredible 716 Hz (Hessels et al., 2006). It was discovered recently using the Green Bank Radio Telescope (GBT) in the dense globular cluster Terzan 5. At the other end of the spectrum lies PSR J2144-3933, rotating with a period of only 8.51 s (Young et al., 1999). Between those two extremes lie more than 1600 pulsars. The bimodal character of the distribution in spin frequency (figure 1.1) suggests the existence of 2 distinct populations of pulsars. The population of *normal pulsars* has longer periods and is well separated from the short-period *millisecond pulsars* (MSPs). The first MSP to be discovered, PSR B1937+21 (Backer et al., 1982), held the title of the fastest pulsar for more then 20 years before being displaced to second place by Ter5ad.
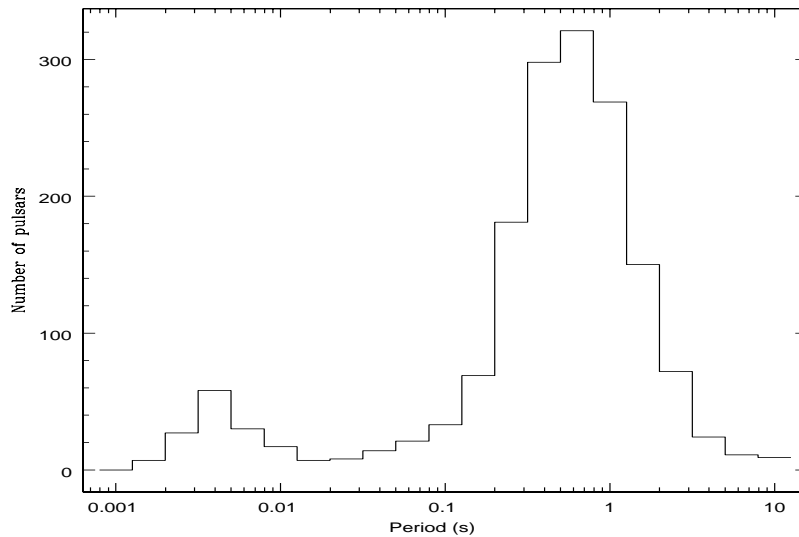
Figure 1.1: Bimodality in the distribution of pulse period for ~ 1600 known pulsars clearly suggest the existence of 2 distinct populations. Data from the ATNF pulsar Catalogue (Manchester et al., 2005, http://www.atnf.csiro.au/research/pulsar/psrcat/).

Binary pulsars The question we need to answer now is: "What process is responsible for the creation of millisecond pulsars?" Before we can answer the question, a few words must be said on pulsars in binary systems for they are the likely bridge between normal and millisecond pulsars. The simplest evolutionary scenario by which a binary pulsar can be created starts with two main sequence stars orbiting each other (e.g., Bhattacharya and van den Heuvel, 1991). The most massive star will evolve off the main sequence first and eventually explode in a supernova to form a neutron star. Many variations on this theme exist where the initial masses of the two stars dictate the details of the different evolutionary scenarios as well as the characteristics of the resulting binary systems (e.g. Stairs, 2004). Many binary systems will be disrupted by the initial kick imparted to the neutron star by the supernova but some systems will remain bound.

Following the creation of the neutron star, the companion star will eventually evolve off the main sequence and become a red giant. Depending on the orbital parameters of the surviving systems, the gravitational field of the pulsar may start attracting matter from its

companion. In the standard *recycling model* (e.g. Alpar et al., 1982), the in-falling matter will form an accretion disk which will transfer angular momentum from the companion star to the neutron star. Such systems are usually visible in the X-ray. The process will result in the spinning up of the pulsar as well as in a significant reduction in its magnetic field strength (Bisnovatyi-Kogan and Komberg, 1974). The main difference between these *recycled* pulsars and the normal pulsars, beside their spin periods, reside in their spin-down rates. It can be seen from the $P - \dot{P}$ diagram (figure 1.2) that the recycled pulsars will migrate from the main population of normal pulsars to the lower left corner of the diagram.

The recycling period will not, however, last forever. If the secondary star is not massive enough to undergo a supernova, the accretion period will usually last a significant amount of time, and the pulsar will be spun-up to millisecond periods while the companion star evolves to eventually become a white dwarf (WD). On the contrary, if the secondary star is massive enough to undergo a supernova explosion and form a second neutron star, the result, provided that the system remain bounds, is a rare double neutron star binary. A famous example of this scenario is the double-pulsar binary J0737-3039 (Burgay et al., 2003; Lyne et al., 2004).
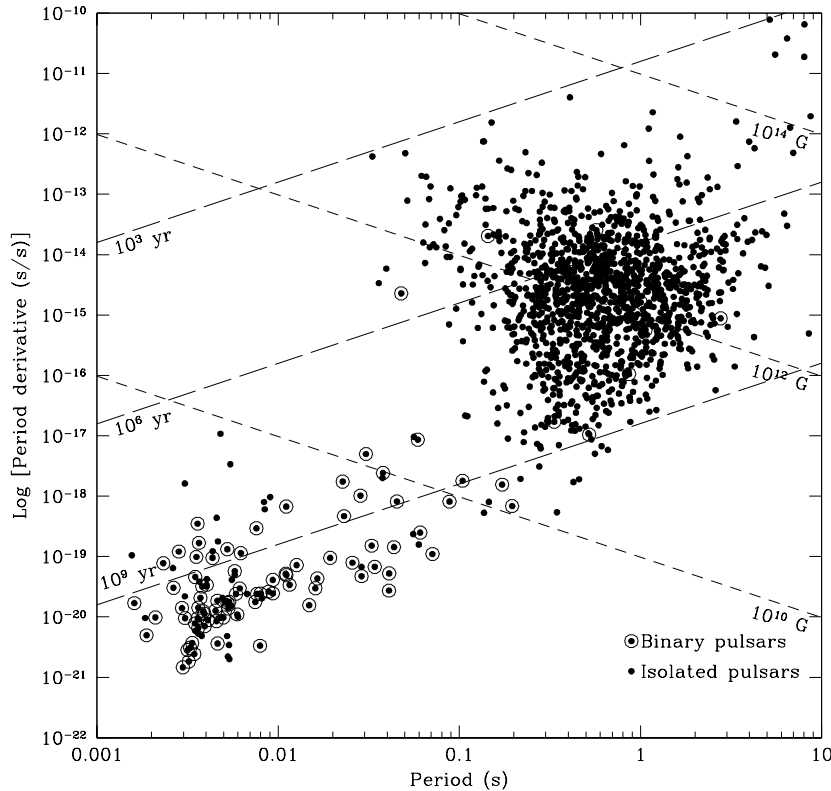
Figure 1.2: The $P - \dot{P}$ diagram highlight the 2 populations of pulsars. Members of binary systems are highlighted by a circle. Also shown are lines of constant magnetic field and characteristic age. Data from the ATNF pulsar Catalogue (Manchester et al., 2005, http://www.atnf.csiro.au/research/pulsar/psrcat/).

1.3   Globular Clusters

Globular clusters are spherical collections of stars associated with the Galaxy. They contain between ten thousand to a few million stars very tightly bound by gravity, which gives them their spherical shape. The size of globular clusters is not trivial to define and takes many forms. The radius at which the stars are tidally pulled away by the Milky Way is called the tidal radius (r_t). Another useful definition is the cluster half-mass radius (r_m) defined as the distance from the core containing half the mass of the cluster. Finally, the core radius (r_c) of the cluster is the distance from the center where the light surface density as seen from the Earth is half of the central value. Typical values for the radii are 50 pc, 10 pc and 1.5 pc respectively (Padmanabhan, 2001; Binney and Tremaine, 1987). Conveniently, given that GCs are relatively far away, these radii usually translate into angular dimensions that fit within the beam of our radio telescopes. According to the globular cluster catalogue maintained by Harris (1996), there are currently about 150 known Milky Way globular clusters.

Figure 1.3: Infrared image of the globular cluster M28 from the 2MASS atlas (credit: Atlas Image courtesy of 2MASS/UMass/IPAC-Caltech/NASA/NSF). M28 was the first globular cluster where a millisecond pulsar, PSR B1821-24A, was discovered (Lyne et al., 1987).

1.3.1   Why do we expect exotic pulsars in Globular Clusters?

The first globular cluster millisecond pulsar was discovered in 1987 (Lyne et al., 1987) in M28 (NGC 6626). PSR B1821-24A is an isolated pulsar with a rotation period of 3 milliseconds. Since then, more than 129 pulsars have been discovered in 24 globular clusters (see http://www2.naic.edu/~pfreire/GCpsr.html for an up-to-date catalogue), including those presented here.

There are many differences between the pulsars in globular clusters and those in the field. The first thing to notice is the sheer number of MSPs in globular clusters with only 6 slow pulsars (P $\geq$ 100 ms) where most of the pulsars in the field have P $\geq$ 100 ms (see

Fig. 1.1). The orbital periods of globular cluster binary pulsars tends to be shorter than those in the field and their orbital eccentricities are usually larger. There is also a greater proportion of isolated millisecond pulsars in clusters.

The extremely high stellar density in the cores of globular clusters results in stellar interactions which might be responsible for the differences between the two populations. Mass segregation caused by dynamical friction in the globular cluster as well as the high mass of the neutron stars imply that pulsars should usually reside near the GC core. In the crowded environment typical of the globular cluster cores, dynamical interactions are likely to play a significant role in the formation of the observed pulsars. During the lifetime of the globular clusters ($\sim 10^{10}$ yrs), the neutron stars are likely to interact with many stars, leading to a rate of production rate of low-mass X-ray binaries which is markedly higher than in the rest of the Milky Way. Because this has been known for some time now (Clark, 1975) and the *recycling model* connecting LMXB with millisecond pulsars is now widely accepted, globular clusters are a prime target for pulsar searches.

The production (or destruction) of binary systems or the exchange, in existing binaries, of members (e.g., Meylan and Heggie, 1997) can be explained by various types of interactions. In globular clusters with extremely high central density, like the core-collapsed M15, the occurrence of physical collisions must be relatively high. Hydrodynamic simulations (Rasio and Shapiro, 1991; Davies et al., 1992) of such a scenario show that collisions resulting in the complete destruction of the companion star could explain the formation of part of the large population of isolated millisecond pulsars (Krolik et al., 1984) or the existence of highly eccentric neutron star - white dwarf binaries when the companion star survives the encounter.

Another interesting scenario is the case where a single neutron star interacts with a primordial binary and acquires a companion through the process of an exchange interaction. Because of the large cross-section of this process and the significant population of primordial binaries in globular clusters (Hut et al., 1992), this could be the most important binary formation process. The properties of the resulting binary seem to be highly dependent on the mass of the acquired companion. If it has a mass $\leq 1 \ M_\odot$, a period of stable mass transfer, following the exchange, will circularize the orbit and lead to a binary system composed of a recycled millisecond pulsar and a white dwarf (e.g. Rappaport et al., 1995). For a main sequence star with mass up to $\sim 3 M_\odot$, the exchanges will lead to intermediate-mass binaries (Davies and Hansen, 1998). Stellar evolution will then drive the binary in a (usually unstable) common envelope phase (Taam and Sandquist, 2000) leading to a binary system composed of a mildly recycled neutron star and a high mass white dwarf with a short orbital period.

Probably the most exotic system would be a binary in which the pulsar orbits a black hole. In this case, a millisecond pulsar, recycled by accretion of matter from a low-mass star, exchanges the white dwarf remnant of that star for a black hole. Such a system has yet to be found but may be discovered in the near future (Sigurdsson, 2003) and is a strong motivator for our searches.

1.3.2 Why study pulsars in globular clusters?

While those exotic systems are interesting in themselves, they also yield extremely valuable information about their host clusters and the physics of neutron stars. With relativistic double neutron star systems such as PSR B2127+11C in the globular cluster M15 (Jacoby et al., 2006), precise measurement of the masses is possible as well as measurement of multiple post-Keplerian parameters leading to a consistency test of the theory of general relativity (e.g. Stairs, 2003). Studying eclipsing binaries like the recently found M28H and NGC6440D (presented in this work) can lead to information on pulsar winds, the nature of

the companion stars and of course the eclipsing mechanisms themselves. Eccentric binaries like some of the new MSPs found in M28 (C and D) and NGC6440B and extremely fast rotators like Ter5ad (the fastest known pulsar)(Hessels et al., 2006) might help constrain the equation of state of matter at supra-nuclear densities.

Globular cluster pulsars can also be used as a sensitive probes into the nature of the clusters in which they reside. For example, they have recently been used to probe properties such as the mass-to-light ratios in the core of NGC 6752 (D'Amico et al., 2002) and 47 Tucanae (Freire et al., 2001a). Timing the millisecond pulsars in 47 Tuc also resulted in the first detection its ionized gas content as well as the cluster proper motion (Freire et al., 2003).

1.4 Aim of this Thesis

In order to do all this science, one must first find some pulsars. The first objective of this thesis was therefore to conduct deep searches of several globular clusters and try to find new normal, millisecond or binary pulsars. By doing so, not only are we making a contribution by increasing the known number of pulsars but we are also trying to answer questions such as how many pulsars reside in clusters? Because of the incredible quality of the instruments used to conducted the searches, finding a new *fastest* pulsar or other exotic type of pulsars was well within our capabilities.

The second objective was to infer properties of two globular clusters (M28 and NGC 6440) from their population of pulsars.

Chapter 2

Searching for Millisecond Pulsars in Globular Clusters

When searching for millisecond pulsar in globular clusters, one must face a number of challenges coming from the interstellar medium as well as from the nature of the pulsars themselves. To observe radio pulsars, we collect data in the form of a time series recorded at a certain sampling rate at a particular frequency. Because they are very weak radio sources, individual pulses in the time series are visible only from the strongest pulsars. For all the other pulsars, including our new discoveries, the signal is well hidden within the background noise. The task, which is conceptually simple, is to find dispersed signals of unknown pulse period, dispersion measure and possibly acceleration in noisy data.

In this chapter, I will first discuss the various issues that must be taken into consideration to conduct successfully a globular cluster pulsar search survey. I will then describe the telescope and the instruments that were used and finally present the standard search procedure as well as some details relevant to our survey.

2.1 The issues

Pulsars are usually very faint radio sources with steep spectra (stronger at low frequency) that can usually be described by a simple power law $S_\nu \propto \nu^\alpha$ where the spectral index has an average value $\alpha \sim -1.8$ (Maron et al., 2000a). It is therefore important to use a telescope with a large collecting area and instruments able to record data across a wide bandwidth, especially at high frequency. Because of the high stellar density in globular clusters and the enhanced likelihood of interactions between the stars, a large proportion of the pulsar population is likely to be in binary systems. Orbital motion during long integrations usually results in a change in the apparent spin period of a binary pulsar (Fig. 2.1). This change translates into the spreading of power in the Fourier domain, thereby reducing the apparent signal-to-noise ratio of a periodic signal and reducing our ability to detect it. If this issue is not dealt with, many relatively bright binary pulsars could remain undetected. Also, millisecond pulsars can have spin periods at least as fast as 1.39 ms (Hessels et al., 2006) with a pulsed signal covering only a small fraction of that time. In order to maintain reasonable sensitivity, we need instruments with a high time resolution and a fast sampling rate.

The dispersion from the interstellar medium causes smearing of the signal across the bandwidth. The amount of dispersion depends on the electron content along the line of sight, which is a priori unknown, adding an extra parameter in the search procedure. To fight this dispersive smearing effectively requires many channels across the bandpass. The propagating signal is also scattered due to density fluctuations in the interstellar medium. This effect has a strong frequency and distance dependance ($\tau_s \propto \nu^{-4} d^2$) and the smearing can be minimized by observing at high frequency. See the *Handbook of Pulsar Astronomy* (Lorimer and Kramer, 2005) for a detailed discussion.

More problems arise from the fact that globular clusters are relatively distant and there-
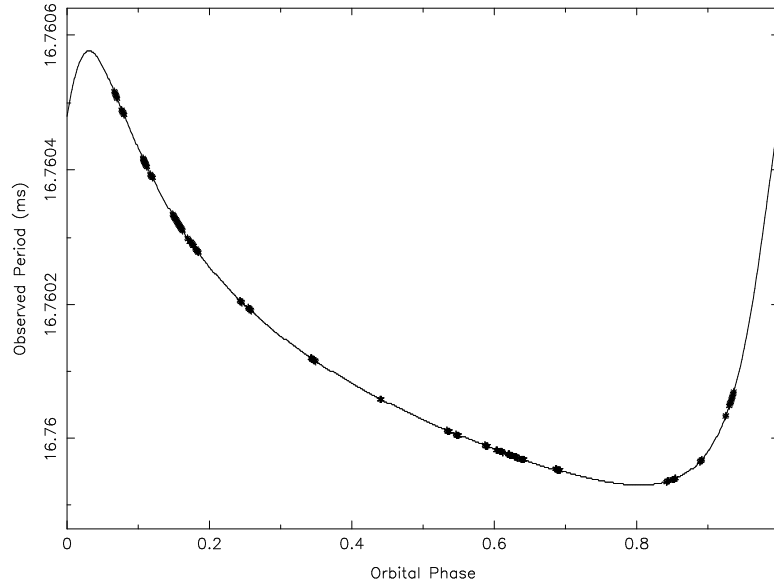
Figure 2.1: The effect of the high eccentricity of NGC6440B on the apparent spin period of the pulsar. The solid line indicates the best-fit orbit.

fore require much longer observation time than typical galactic searches, increasing the complexity of the data reduction phase. On the other hand, globular cluster search campaigns remain possible because of the relatively small number of search targets and the possibility to observe many pulsars at once. For example, there are about 100 globular clusters visible from Green Bank (West Virginia). Leaving behind the ones that are too small or lack the density for the likely formation of millisecond pulsars, we still need a good selection criteria in order to make any survey as successful as possible. For this thesis, I joined a recently begun globular cluster survey using the Green Bank Telescope at S-band (1.95 GHz). In order to choose the best globular cluster candidates, our group used a parameter (Γ_c, see Pooley et al., 2003) indicating the stellar interaction rate in the core of the cluster. We believe that this parameter is a good indicator of the present rate of millisecond pulsar formation which should be correlated with the total number of MSPs in the cluster.

My main collaborators on this survey were Scott Ransom (NRAO), Paulo Freire (NAIC), Jason Hessels (McGill) and my supervisor, Ingrid Stairs.

2.2 Data acquisition using the Green Bank Telescope (GBT)

Most of the issues mentioned in 2.1 can be overcome using state of the art instruments and software. All the observations in this project were made using the National Radio Astronomy Observatory's 100-meter Green Bank Telescope (GBT) with the Pulsar Spigot backend (Kaplan et al., 2005) or the Berkeley-Caltech Pulsar Machine (BCPM) (Backer et al., 1997). The large collecting area of the GBT and its ability to view, with an unblocked aperture, the entire sky above 5 degrees elevation, makes it a tool of choice for pulsar astronomy.

My first task in this project was to analyze some data taken in 2001 during some of the first scientific observations made using the Green Bank Telescope. These observations

were part of a 20-cm (L-band) survey for pulsars in globular clusters using both the GBT and the Arecibo Telescope (Ransom et al., 2005). A number of globular clusters were observed using the GBT at L-band with the Berkeley-Caltech Pulsar Machine which operate as a digital filter bank. The BCPM data was typically sampled every 50 μs and written with 4-bit precision and 96 channels across a 130 MHz bandwidth centered at 1375 MHz. Unfortunately, the data were plagued by a lot of broadband interference, greatly reducing our sensitivity to weak pulsars. My part was to analyze some data on one of the observed clusters, M4, and although the search did not lead to the discovery of new pulsars, it was a very good learning experience.

Following the BCPM analysis, I became involved with a more recent globular cluster pulsar survey at S-band using the GBT with the Spigot backend (proposals GBT 05B-028 and GBT 05C-056). The choice of S-band for the survey is motivated by the huge success of a previous survey on Terzan 5 (Ransom et al., 2005), the relatively radio-frequency-interference (RFI) clean 600 MHz of band between 1650 and 2550 MHz, and the low system temperature of the GBT receiver in this range. The Spigot backend is a new instrument (Kaplan et al., 2005), specifically designed for pulsar searching and timing (see Tab. 2.1 for a comparison). The Spigot card is built around the GBT autocorrelation spectrometer and is available in a number of modes. In our mode of choice and in the absence of heavy scattering, we remain sensitive to sub-millisecond pulsars (see section 2.6). For example, at a DM of 220 cm^{-3} pc, the short sampling time (81.92 μs) and large number of channels across the bandpass (768) represent a dispersive smearing across 1 channel of only 89 μs at 2 GHz. We used the Spigot in mode 2 where the signal is digitized with three levels, autocorrelated and recorded with 16-bit precision.

Unfortunately, the data rates are large, making storage and processing of the data difficult. The data, which comes at the rate of 85.8 GB hr^{-1}, is written to disk in the standard FITS format on a computer with four 1 TB RAID systems. In order to save precious disk space and because we usually know the nominal DM of the observed globular clusters, we usually partially dedisperse the data on the Spigot computer. We then either write the data to one of our many external disks or transfer it to a different computer via a high-speed direct ethernet connection. The reduction of the data, which we describe later, can then be performed on dedicated clusters in Charlottesville at NRAO (Uller) or in Vancouver at UBC (Oak).

For the globular cluster M28, we also had access to some data taken with the Parkes telescope in 2003. The data were taken with the central beam of the multibeam system, sampled every 80.0 μs and written with 1-bit precision. The observations were made at L-band using 512 channels across a 256 MHz bandwidth centered at 1375 MHz. The data were kindly provided to our collaboration by Haydon Knight.

	T_{obs} (min)	ν_c (MHz)	$\Delta\nu$ (MHz)	N_{chan}	t_{samp} (μs)	Bits
Spigot	180	1950.0	600	768	81.92	16
BCPM	240	1375.0	134.4	96	50.0	4
Parkes (fb)	240	1375.0	256	512	80.0	1

Table 2.1: Details of the 2 instruments used to conduct the observations for this project. Most of the data was taken using the GBT + Spigot (mode 2) but some early data using the GBT + BCPM was also analyzed.

Over the course of this project, we have collected over 200 hours of data on the 3 globular clusters M28, NGC6440 and NGC6441 plus a few early observations of NGC6522

and NGC6624. I estimate my personal contribution the the data collection to ∼30%. To date, I have processed and conducted acceleration searches on about 70% of those ∼17,000 GB of data and found 7 of the 23 new pulsars reported in this work. Table 2.2 summarizes the observation details.

Cluster	Date range	Number of observations	Observing time (hrs)	Fraction of the data searched
M28	Sept 2005 - Sept 2006	22	63.3	71%
NGC6440	April 2005 - Sept 2006	25	70.0	63%
NGC6441	April 2005 - Sept 2006	25	61.0	63%
NGC6522	Sept 2005	1	7.0	100%
NGC6624	July 2005	1	6.4	100%

Table 2.2: Details of the observation of 5 globular clusters using the GBT + Spigot (mode 2) during the course of this project. The last column report an estimate of the total fraction of the collected data that has been processed and searched by the members of our collaboration.

2.3 Dispersion measure

2.3.1 Propagation through a homogeneous medium

The interstellar medium (ISM) can be described as a cold ionized plasma. When electromagnetic radiation travels through the ISM, its propagation is affected by a frequency-dependent index of refraction. This will result in the dispersion of the pulse of an incoming pulsar signal traversing the ISM. It was first observed by Hewish and his collaborators in their discovery of pulsars (Hewish et al., 1968).

While the mechanism by which the pulsar emits radio waves is still unclear, it is usually assumed that an emission cone, located at the magnetic pole of the neutron star, emits the radio pulses simultaneously at all frequencies within a large bandwidth. As they propagate through the ISM, radio waves are affected by the frequency dependence of their group velocity. Pulses emitted at lower frequencies travel with slower speeds through the interstellar medium, therefore arriving later than those emitted at higher frequencies (Hankins and Rickett, 1975). The time delay Δt between the arrival time of two pulses is related to their observing frequencies f_1 and f_2 (in MHz)

$$\Delta t = \frac{1}{2.41 \times 10^{-4}} \times \left(f_1^{-2} - f_2^{-2}\right) \times \mathrm{DM} \text{ s} \tag{2.1}$$

where the constant of proportionality labeled DM is called the *dispersion measure*. It is the integrated column density of free electrons along the line of sight

$$\mathrm{DM} = \int_0^d n_e dl \tag{2.2}$$

and is usually expressed in cm^{-3} pc. Given a model of electron density and a measurement of the DM, it is possible to obtain a crude estimate of the pulsar distance (e.g. Cordes and Lazio, 2002).

2.3.2 Dedispersion

When a pulsar with a high DM (which is often the case with globular cluster pulsars) is observed using a receiver with a high bandwidth, the pulse will be smeared and the peak

intensity reduced (Fig. 2.2). There is, however, a simple way to compensate for the effects of dispersion. Using a spectrometer, we can split the bandwidth into a large number of independent frequency channels. We can then apply a time correction on each channel for the relative delay between the pulses at different frequencies. This process, which is called *incoherent dedispersion*, can greatly improve the signal-to-noise. It can be carried out using dedicated hardware but is usually dealt with at the software level. By adding all the properly delayed frequency channels together, we produce a *dedispersed time series* which can then be searched for periodicities.
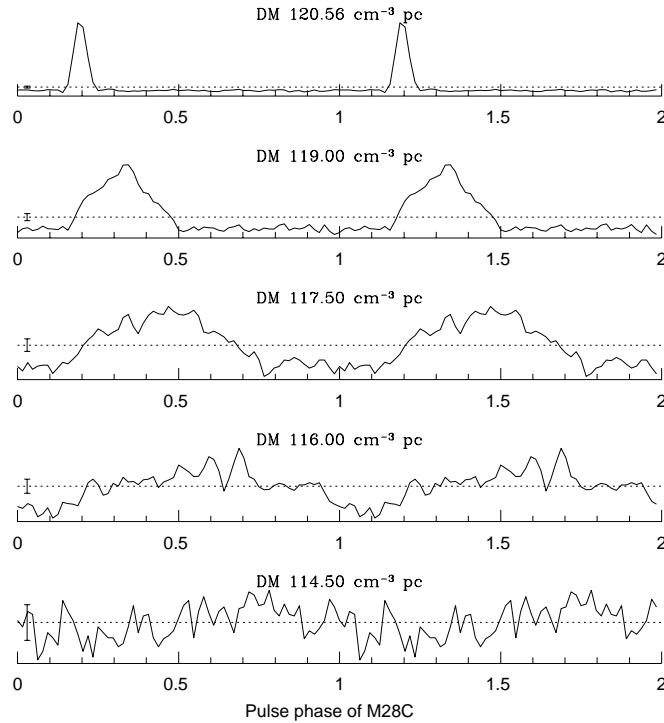
Figure 2.2: The effect of folding the pulsar M28C at the wrong value of dispersion measure is evident on the signal-to-noise ratio. The dotted line and vertical bar on the left represent the profile average and standard deviation respectively. The top plot was folded using the correct value of DM.

In general, when searching for pulsars, the dispersion measure is not known and the DM space must also be explored. The common procedure is to produce dedispersed time series for a large number of trial DMs which are then searched for periodicities. For globular cluster pulsars, we have an advantage because their dispersion measures will all be similar; still we must be careful to sample finely enough to detect pulsars with a DM between two trial values. The typical DM step size used in this survey was ΔDM = 0.5 cm^{-3} pc. The impact of using the wrong DM to fold a pulsar can be quite dramatic as is illustrated in Figs. 2.2 and 2.3.

The frequency dispersion of pulse arrival time for a typical observation of a pulsar with a DM of 200 cm^{-3} pc using the GBT + Spigot is only Δt = 0.175 ms between 2 channels. Once a pulsar is found in a globular cluster, its dispersion measure can be used to constraint
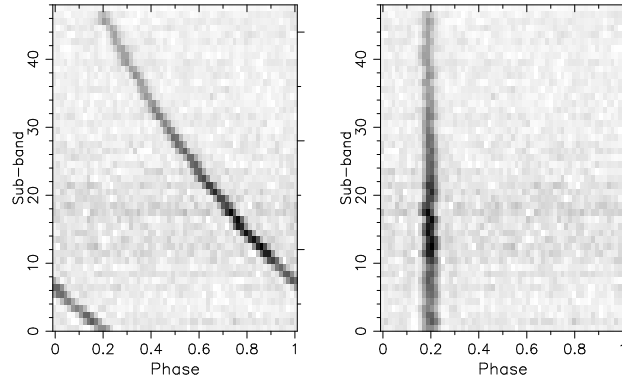
Figure 2.3: The grey-scale plots shows the pulse phase as a function of frequency. The total bandwidth is split into many subbands which have each been previously dedispersed at the nominal DM value for the host globular cluster. The left side shows the pulsar M28C folded at the wrong DM of 114.00 cm^{-3} pc and on the right side at the correct DM of 120.56 cm^{-3} pc. By choosing the correct DM we introduce time delays between the subbands that align the pulse phase in frequency. The delays are calculated from the center frequency of the channels and the value of the DM (eq. 2.1). The stronger signal and background between the subbands 10 and 20 is due to the shape of the bandpass.

the DM space in later searches. Typically, all the pulsars in a globular cluster have a DM which is not very far from the nominal value of the cluster DM known from the first pulsar. This value can be refined later as we keep finding more pulsars. A common practice is to use this value of DM to create subbands. By doing that we introduce, as discussed in 2.6, a certain amount of smearing but we also reduce drastically the amount of data to be stored. By summing all the frequencies within a subband of bandwidth $\Delta\nu$, the pulse will be smeared over a time interval

$$\tau_{DM} = 8.3 \times 10^3 \; \frac{\Delta DM}{\nu_{MHz}^3} \; \Delta\nu \; \text{sec} \tag{2.3}$$

where ΔDM is the difference between the pulsar's real DM and the DM used to create the subbands and ν the central frequency of the subband (Lyne and Smith, 1998).

2.3.3 Method: data preparation

All the data was analyzed using a suite of software called PRESTO[1] (Ransom, 2000). The software package is composed of a number of routines that are designed to search for pulsars. I will now describe the first stage of a pulsar search analysis.

RFI excision Radio frequency interference (RFI) is considered to be the bane of radio astronomy. RFI can arise from persistent broadband signal from sources like the Lynchburg airport radar system ($P \simeq 12$ s) close to the GBT or electrical devices such as the AC power lines ($\nu = 60$ Hz). Persistent sources are annoying mainly because they reduce the available bandpass but are somewhat easier to deal with due to their predictability. Transient sources like an electrical storm or a passing satellite are a lot more difficult to remove. In any case,

---

[1]available from http://www.cv.nrao.edu/~sransom/presto/

RFI has to be dealt with or else the list of candidates from the search software could become unmanageably long or worse, a real pulsar could not even be recorded as one.

In this survey, RFI excision was done using *rfifind*. This routine searches for interference in the raw data both in the time and frequency domain and returns a *mask* that can be used to remove portions of the data. Unfortunately, this is a computationally expensive stage and the mask would often propose to remove a significant portion of the data. Therefore, for most observations, a decision has been made not to use rfifind at the expense of more time spent looking at RFI instead of potentially real candidates.

Instead, RFI has been dealt with at later stages in the search procedure. First, a list of known periodic RFI sources (*birdies*) was used to remove strong signals from the Fourier spectrum but most of the RFI was filtered out by visual inspection of the search results. The 2 methods are described later in the text.

Dedispersion   The raw data is then dedispersed in a number of subbands (usually 48 over 600 MHz) at the nominal DM of the searched globular cluster using *prepsubband*. From the subbands we then create 40 (typically) dedispersed time series covering a range of trial DMs which depends on the choice of DM steps. Because we are analyzing deep observations, the effects of the rotation of the Earth and its motion around the Sun have to be corrected for prior to any periodicity search. The topocentric data (as observed at the telescope) is then referred to the solar system barycenter which can be considered an inertial frame. Barycentring is done by prepsubband via TEMPO (more on TEMPO in chap. 3). The number of points in the time series is also adjusted, either by padding or truncating, such that it factorizes so that the largest prime factor is small. Although not necessary, this usually results in a net improvement in computation time.

Fourier transform   The last step of the data preparation consists of the Fast Fourier Transform (FFT) of the all dedispersed time series. Depending on the length of the time series, the transformation is performed either in-core or out-of-core (see Ransom et al., 2002, for more details). The known birdies are removed at this stage using *zapbirds*. This routine removes known sources of interference from the Fourier transform of a dedispersed time series by replacing them with the local average Fourier amplitudes. The list of frequencies to zap is usually built by exploring the Fourier transform of a topocentric time series dedispersed with a DM of 0 and looking for strong signals. Any signals of terrestrial origin will not be significantly dispersed before being detected by the telescope. The central frequency of the RFI signals as well as their width (in fourier bins) and the number of harmonics to zap are listed in a *birdie* file. To save some time at the candidate sorting phase, previously known pulsars that are particularly strong (e.g M28A) are also listed and zapped from the FFT.

2.4   Search for periodicities

One of the standard pulsar search techniques makes use of the Fast Fourier Transform of a dedispersed time series to look for unknown periodic signals in the frequency domain (for more details see Lorimer and Kramer, 2005). Such techniques are very successful at finding periodic signals in noisy data but suffer from reduced sensitivity for pulsars in binary systems with short orbital periods. Standard frequency domain analysis works under the assumption that the apparent pulse period remains constant throughout the observation, an assumption that is only valid for isolated pulsars or binary pulsars with orbital periods much longer than the integration time. The effect of the binary motion is to distribute the Fourier power over many frequency bins by changing the apparent period of the pulsars during the observation. The Doppler-shift of the pulse frequency usually results in the smearing of spectral features

and a drastic reduction in the signal-to-noise (Johnston and Kulkarni, 1991). Those search techniques are definitely not suitable for a globular cluster survey where we are expecting to find pulsars in binary systems and where integration times are typically many hours.

Many methods have been developed to try to recover the loss in sensitivity. One such technique involves the resampling of the time series to the rest frame of an observer inertial with respect to the pulsar. By assuming that the pulsar has a constant acceleration during the observation, the time series is stretched using the Doppler formula for a number of trial accelerations (Middleditch and Kristian, 1984). An accelerated pulsar will then appear to have a constant period and the spectral features will be unbroadened. This method has seen some success for pulsar searches in the globular cluster 47 Tucanae (Camilo et al., 2000) but the extra search parameter coupled with the fact that a FFT must be performed for each trial acceleration quickly makes this approach computationally too expensive for long data sets.

A few methods working in the frequency domain are worth mentioning. The Dynamic Power Spectrum technique has been used successfully by a few groups (e.g. Chandler, 2003). Phase-modulation searches (Ransom et al., 2003), implemented in the routine *search_bin* in PRESTO, is a very promising new technique specifically designed to search for binary systems with orbital period comparable or much less than the integration time. This method has been used to analyze some of the data in this project but no pulsars were found.

2.4.1   Method: frequency domain acceleration search

The search technique that was used in this thesis is implemented in the routine *accelsearch* in PRESTO. It is a more efficient approach than the time domain acceleration search. By working entirely in the frequency domain, only one FFT needs to be performed per dedispersed time series. The so-called *correlation* method allows a fully coherent search in acceleration space that is equivalent to the time domain resampling but is computationally much cheaper. The acceleration ($\dot{\nu}$) is assumed to be constant over the course of the observation and is parametrized in the Fourier domain by $\dot{r} = \dot{\nu}\mathrm{T}^2$ where T is the length of the observation. For details on the method and its implementation in PRESTO, see Ransom et al. (2002).

The technique is also useful in finding isolated pulsars since for time series of very long duration, even the very small spin-down of a pulsar can cause a signal to drift across a number of Fourier bins. It has an optimal sensitivity for pulsars in binary systems with an orbital period that is much longer than the observation time ($\mathrm{P}_B \geq 10\times\mathrm{T}_{obs}$) (Ransom et al., 2002). For this reason, the acceleration searches were performed on all the observations as a whole as well as on overlapping segments of various shorter durations (typically 55 and 95 minutes). The searches were also conducted over two ranges of Fourier frequency derivative $\dot{r}$ usually covering -4 $\geq \dot{r} \geq$ 4 and -400 $\geq \dot{r} \geq$ 400.

Another feature of accelsearch is the ability to do the incoherent addition of a specified number of harmonics. The technique of harmonic summing (Taylor and Huguenin, 1969) is present in nearly all modern search techniques as a mean to increase the sensitivity to narrow pulses. Depending on the duty cycle of the pulse, its power in the Fourier domain will be distributed between the fundamental frequency and a number of harmonics. To perform harmonic summing, the original spectrum is stretched by a factor of 2, 4, etc. and then added to the original spectrum, increasing the S/N of the narrow pulse. For a pulse with a duty cycle of 5%, adding 8 harmonics would suffice but for narrower pulses, up to 32 harmonics may be summed to improve the sensitivity (Ransom et al., 2002).

2.5 Sorting the candidates and folding of the good contenders

The search routines in PRESTO return their results in the form of a list of candidates. For a chosen range in acceleration parameter, one such list is produced for every dedispersed time series. So for a typical search on a long observation (say 4 hours), 80 candidate files would have to be investigated for the full scan search and 480 files resulting from the search on shorter segments. The candidates are organized in order of decreasing significance σ (the σ reported by PRESTO is not S/N but the equivalent gaussian significance of measuring that signal; for more details see Ransom et al. (2002)). For each candidate, information such as the coherent power (calculated by adding the Fourier components in phase), the apparent frequency and frequency derivative or the number of harmonics summed is given. Each file can contain anywhere between several tens to a few hundred candidates. Extracting the good candidates is a non-trivial task which can not be efficiently done by looking at each candidate. Fortunately, a few tricks can be used to reduce the number of candidates to a more manageable level.

Candidate optimization The first step is to look quickly through all the candidates. By sorting them in order of increasing pulse period, candidates that appear at all DMs without a significant change in σ or coherent power can be ignored as they probably are of terrestrial origin. On the other hand, if a signal is from a pulsar, the significance of that particular candidate would appear to peak at a particular DM. Most of the bright pulsars in a globular cluster can usually be identified in such a way; for all the others, a more thorough approach is necessary.

A python script called *sift_better.py* (part of the PRESTO package) was used to examine the candidate files from a particular search and return only those passing certain tests. The first level of filtering is done by keeping only the candidates with a σ or a coherent power above a certain value (usually $\sigma \geq 2$ or coherent power ≥ 100). There is also no need to investigate candidates that are close enough in Fourier bin to be considered the same (duplicates). From the several thousands of candidates that usually pass one of the two threshold tests, *only* several hundreds usually remain after the duplicates removal in the case of a full integration search and a few thousands for the search on short segments.

Folding The next step consists in the visual inspection of the remaining candidates. As mentioned before, the individual pulses can rarely be seen in a time series. In order to see them above the noise level, we must perform the coherent addition of many pulses together, a process called *folding*. By doing so, we produce an *integrated profile* which can then be inspected and, when revealing a real pulsar, used to extract useful information about the pulsar and its surroundings. By adding the pulses modulo the pulse period, the signal will grow roughly linearly with the number of pulses (n_p) while the noise increases as the square root of the number of pulses. Since the number of pulses is directly proportional to the observing time, the resulting signal-to-noise ratio is: $\mathrm{S/N} \propto \sqrt{n_p} \propto \sqrt{t}$.

The folding of the best candidates is done by a routine called *prepfold* implemented in PRESTO. Prepfold can produce two different plots containing various amounts of information. When used to fold raw radio data or subbands (Fig. 2.4), prepfold will explore the DM space as well as search over a range of pulse periods and period derivatives around the values given as input and produce an optimized pulse profile. In that case, the plot contains the folded profile, a grey-scale plot of pulse phase as a function of time and of phase as a function of the observed frequency. It also contains plots of reduced χ^2 as a function of DM, pulse period and period derivative and a 2-D plot of the $P - \dot{P}$ space explored by

prepfold. Unfortunately, the value of the reduced χ^2 reported by prepfold is contaminated by a procedure used during the observations in which the signal level is adjusted every few tens of seconds in order to reduce the risk of overflow. Because of that, the absolute value of χ^2 usually has no real significance in itself for most of our observations. A different fold can be created by using a dedispersed time series as input (Fig. 2.5). In this case, prepfold will not search in DM space and the output plot does not contain frequency dependant information. This type of fold being much faster, it is therefore suitable for the first level of visual inspection.
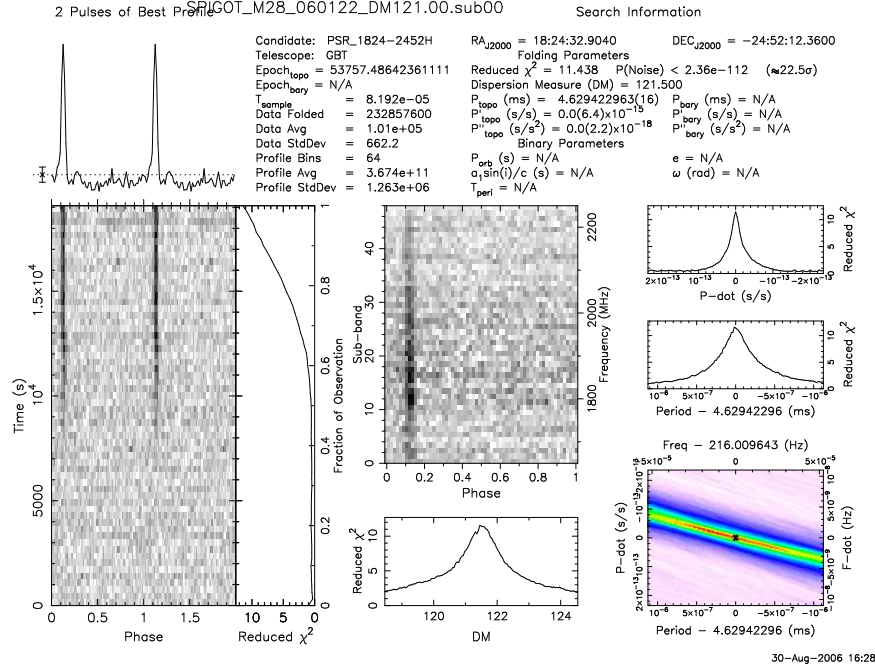
Figure 2.4: Example of a plot produced by prepfold from the subbands. On the left side is the same information as in Fig. 2.5. On the right side, the S/N of the $P - \dot{P}$ space is plotted along with a plot of reduced χ^2 versus DM and a grey-scale plot of pulse phase as a function of the observed frequency. Folded here is M28H, a 4.63 ms pulsar in a binary system discovered recently by Scott Ransom.

Visual inspection   The visual inspection of the folded profiles of all the candidates surviving the optimization phase is time consuming, slightly tedious but nonetheless essential. Over the course of this thesis, over 30,000 plots have been inspected by eye resulting in the discovery of 7 new millisecond pulsars. During the inspection, we look for specific features characteristic of pulsars (Fig. 2.5). If the folded profile shows a clear peak that appears at the same phase for all sub-integrations and the $P - \dot{P}$ plot shows an obvious maximum, then the candidate might be a real pulsar. In some instances, if the signal comes from a pulsar in a binary system exhibiting eclipses, the pulse can disappear for some fraction of the observation. On the other hand, if a signal shows up in only one or very few sub-integrations, odds are that it is from some RFI source.

Very few candidates survive the first level of visual inspection. Those that meet some of the above criteria are saved for the next step in which we fold them using the subbands. This permits us to look for other characteristics of pulsars in the output plots (Fig. 2.4).
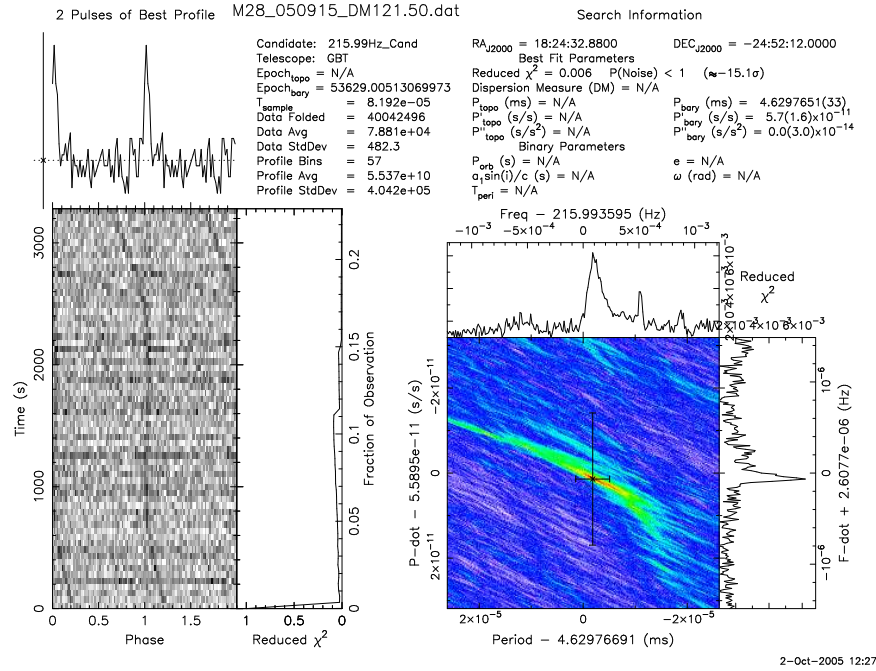
Figure 2.5: Example of a plot produced by prepfold from a dedispersed time series. On the left side is the folded profile above a plot (grayscale) of signal-to-noise for each sub-integrations as a function of phase. On the right side, the S/N of the $P - \dot{P}$ space is plotted. Many plots like this one are inspected by eye for specific features characteristic of pulsars. Folded here is M28H again.

Not only do we require the pulse to appear at the same phase for all sub-integrations, but also for all subbands. If the signal appears only in one or a few subbands, the candidate is discarded as RFI. Finally, the plot of reduced χ^2 versus DM should also have a clear peak. A signal of terrestrial origin would likely peak at zero DM.

Millisecond pulsars in binary systems usually have a different signature than isolated pulsars. As can be seen from Figure 1.2, their spin down rates tend to be smaller but the acceleration from the orbital motion can be (partially) absorbed by the apparent frequency derivative increasing its value by a few orders of magnitude. The signal in the grayscale plot of S/N for time versus phase would likely exhibit a curvature of sorts (as in Fig. 2.5). In such a case, the best period and period derivative found by prepfold might not be sufficient to describe the evolution of the spin frequency within the time of observation. This usually happens when we are trying to fold over the whole observation a candidate that was found in short segments. We can use prepfold to try increasing the S/N by searching for a second period derivative. If that is still not enough to align the peak in phase for all sub-integrations, then a fold on a fraction of the observation will have to suffice. In chapter 3, we will see how we can use timing to create a model that will fold the pulsar on the whole observation. All this procedure may seem like a lot of work for a single candidate, but the pulsars that behave like this are very likely to be from short period binaries, therefore exciting prospects.

Confirmation Usually, when a candidate survives all of the tests mentioned above, we can safely say that we have found a new pulsar. The last test a candidate must pass is its detection in a different data set. Folding a new pulsar on a different observation is

far from trivial, especially in the case of binary pulsars where the acceleration causes the apparent spin period to change between observations. Hopefully, the same pulsar will have been picked up from the acceleration search of a different day and show up in the resulting candidate lists, providing the necessary information for successful folding of the pulsar. If that is not the case, then we can try to find the pulsar again by doing *blind-fold searches*. For a pulsar in a binary system, the apparent frequency and frequency derivative will describe an ellipse (for circular orbit pulsars) or a more complicated shape (for eccentric orbits) in the $f - \dot{f}$ plane (Fig. 2.6) as time progresses (Freire et al., 2001b). The difficulty lies in figuring out the size of the locus on the plane as well as the current position of the pulsar on the path. Using our best guess, we use prepfold to search portions of the plane for a range of trial f and $\dot{f}$ and then do a visual inspection of the resulting plots. If our choice of ranges in the $f - \dot{f}$ plane are too conservative, we run a chance of missing the pulsar, but on the other hand it is clear that the number of plots to inspect can quickly get unmanageable. In the end, it all comes down to how badly you want to find that pulsar again.
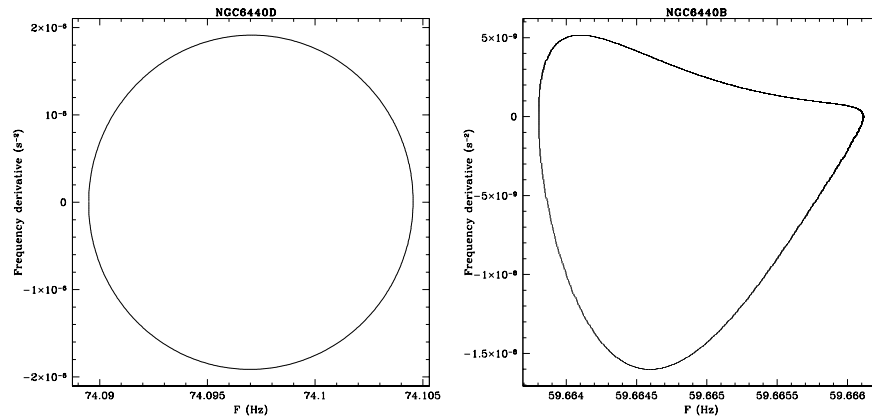
Figure 2.6: The apparent frequency and frequency derivative of the binary pulsar NGC6440D (left panel) describes an ellipse in the $f - \dot{f}$ plane as time progress. On the right panel, the relatively high eccentricity of NGC6440B (e = 0.57) distorts the ellipse significantly. The changes in apparent frequency and frequency derivative have been calculated from the phase connected solutions of both pulsar.

2.6 Sensitivity

The sensitivity of our search is estimated by calculating the minimum flux density, S_{min}, that a pulsar must have in order to be detected. The expression is derived from the radiometer equation (Dicke, 1946), which expresses the root-mean-square fluctuations in system temperature T_{sys} as

$$\Delta T_{sys} = \frac{T_{rec} + T_{sky}}{\sqrt{n_p t_{obs} \Delta \nu}} \tag{2.4}$$

where the S-band receiver temperature is $T_{rec} = 20$ K (value taken from the GBT web site[2]), the sky temperature $T_{sky} = 6$ K (Haslam et al., 1982), the observation time t_{obs} is

---

[2]http://www.gb.nrao.edu/∼fghigo/gbtdoc/sens.html

expressed in seconds, n_p represents the number of summed polarizations and $\Delta\nu$ is the total receiver bandwidth in MHz. Following that, the expression for the minimum flux density is given by (Dewey et al., 1985)

$$S_{min} = \frac{\beta(S/N_{min})T_{sys}}{G\sqrt{n_p t_{obs}\Delta\nu}}\sqrt{\frac{W_{\text{eff}}}{P - W_{\text{eff}}}} \tag{2.5}$$

where the antenna gain is G = 2 K/Jy (value taken from the GBT web site[2]), P is the pulsar period, W_{eff} the effective pulse width and β is a correction factor, of order unity, that accounts for the imperfections due to the digitization of the signal. S/N_{min} is the threshold signal-to-noise of the survey and can be calculated from (Lorimer and Kramer, 2005)

$$S/N_{min} = \frac{\sqrt{ln(n_{trials})} - \sqrt{\pi/4}}{1 - \pi/4} \tag{2.6}$$

where the number of trials for a typical Fourier domain search is calculated from the number of samples, trial DMs and harmonics summed

$$n_{trials} = n_{samples} \times n_{DM} \times [log_2(n_H) + 1]/2 \tag{2.7}$$

For a typical 2 hour observation where 40 trial DMs are searched with summing of 32 harmonics, the signal-to-noise threshold S/N_{min} = 8.35. The calculation of the effective pulse width W_{eff} includes the intrinsic pulse width W_{int}, the effect of dispersion across a single channel t_{DM}, the overall pulse broadening due to the difference between the DM at which the subbands have been created and the true pulsar DM, $t_{\Delta DM}$, and finally, the data sampling interval t_{samp}. Note that the effect of scattering broadening is comparatively negligible at S-band.

$$W_{eff}^2 = W_{int}^2 + t_{DM}^2 + t_{\Delta DM}^2 + t_{samp}^2 \tag{2.8}$$

The calculation of the 2 dispersion broadening effects can be done using equation 2.3. Supposing that the true pulsar DM is off the globular cluster nominal DM by one unit yields $t_{\Delta DM}$ = 10 μs while the sampling time t_{samp} = 81.92 μs. The curves in figure 2.7 are for a pulsar with a 10% duty cycle in 2 globular clusters searched in our survey.

The sensitivity calculations described here do not take into account the degradation in signal-to-noise from the change in the apparent spin period of a binary pulsar due to the orbital motion. This issue was discussed in section 2.4.
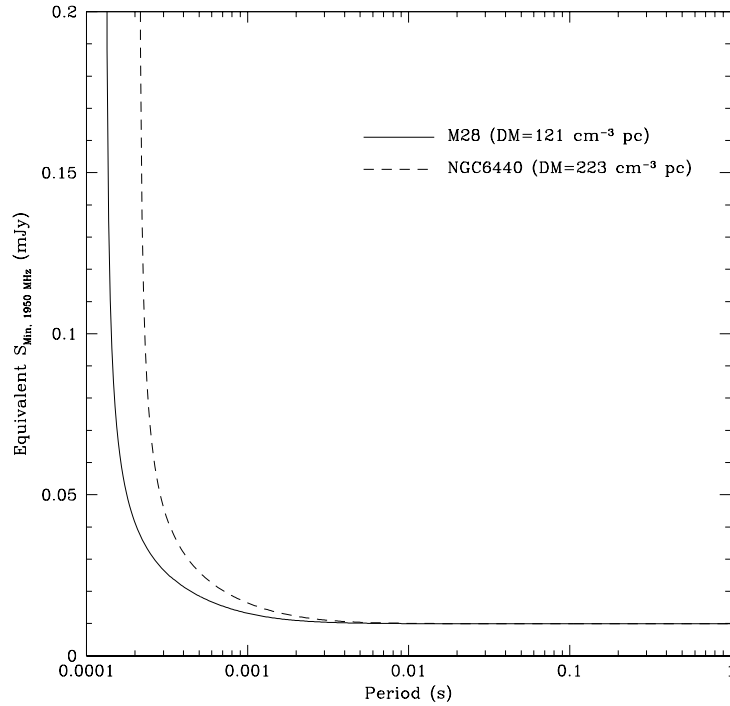
Figure 2.7: Minimum detectable flux density as a function of period for a pulsar with a 10% duty cycle observed for 2 hours with the GBT + SPIGOT, using a 600 MHz band centered at 1950 MHz. The curves are for a pulsar with a true DM one unit away from the nominal DM of 2 globular clusters targeted in our survey. Longer integration times result in even better sensitivity.

Chapter 3

Timing of the new MSPs

We have new pulsars, now what?   The science case for finding new pulsars has been made in chapter 1 and the means by which we find them discussed in the last chapter. We will now address the question of how to extract valuable information from pulsars using a powerful technique called *timing*. Unfortunately, despite the apparent simplicity of the concept and the powerful tools available (e.g. TEMPO[1]), pulsar timing is an 'art' that is difficult to learn. Therefore, this chapter's aim is only to present the general procedure as well as some considerations in trying to obtain phase connected solutions for new pulsars. For a detailed description of the procedure see, for example, Lorimer and Kramer (2005).

3.1   General timing procedure

Pulsar timing consists of the measurement of the times of arrival (TOAs) of the emitted pulses and their subsequent modeling. Our ability to accurately predict future pulse arrival times is a good measure of the quality of a constructed model. To measure pulse arrival times, we must first create a mean pulse profile by folding a dedispersed time series modulo the expected pulse period. TOAs are obtained by cross-correlating the observed profile with a high signal to noise profile used as a template. The TOAs are basically given by the measured time shift between the profile and a reference point on the template along with the time stamp of the observation. High precision in the measurement of the TOAs, which scales as the ratio of the pulse width to the S/N ratio (e.g. Lorimer and Kramer, 2005), is key to the amount of useful information that can be extracted. In this respect, short period millisecond pulsars, with their high rotational stability, generally yield better results than normal pulsars.

$$\sigma_{TOA} \propto \frac{W}{S/N} \tag{3.1}$$

The cross-correlation of the observed profiles with the templates was carried out in the frequency domain using a χ^2 minimization method implemented in the subroutine FFTFIT (Taylor, 1992). This routine is in turn implemented in a python script (*get_TOAs.py*), part of the PRESTO package.

The number of TOAs that could be collected from an observation could, at least in principle, go from 1 to the total number of individual pulses. But because the arrival time of single pulses is not stable and the shape of their profiles changes from pulse to pulse, they are not a suitable choice. Usually, adding a few thousand pulses together is sufficient to ensure that an integrated pulse profile is stable (Helfand et al., 1975). On the other hand, the S/N dependance of the TOA uncertainty (equation 3.1) often suggests much longer integration times, especially for weak pulsars.

---

[1]http://pulsar.princeton.edu/tempo/
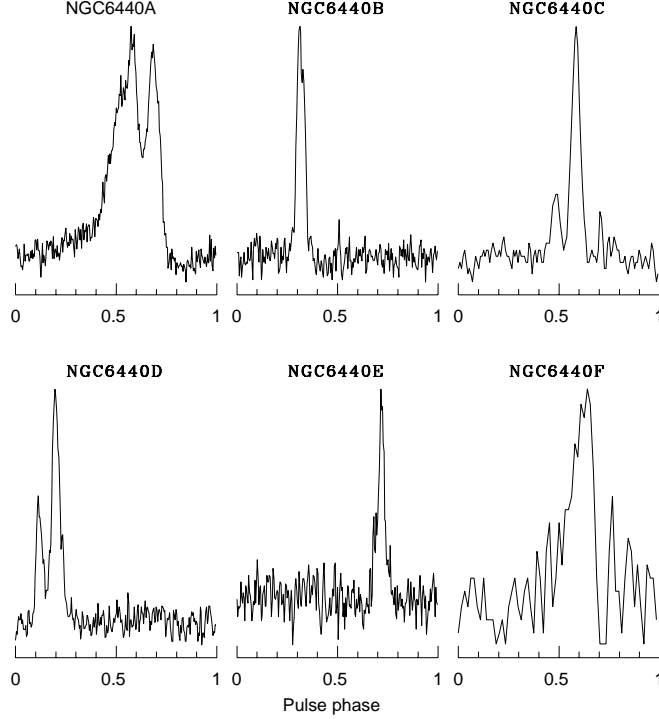
Figure 3.1: The template profiles used to generate TOAs for the timing of the pulsars in NGC6440.

3.1.1 Constructing a timing model

Here we describe the timing fit as implemented in TEMPO. In a reference frame co-moving with the pulsar, we can express the time evolution of the spin frequency using a Taylor expansion

$$\nu(t) = \nu_0 + \dot{\nu}_0(t - t_0) + \frac{1}{2}\ddot{\nu}_0(t - t_0)^2 + ... \tag{3.2}$$

where ν_0 is the spin frequency at a reference time t_0 and $\dot{\nu}_0$ and $\ddot{\nu}_0$ are time derivatives. Integrating equation 3.2 leads to an important component in the construction of a timing model

$$N(t) = N_0 + \nu_0(t - t_0) + \frac{1}{2}\dot{\nu}_0(t - t_0)^2 + \frac{1}{6}\ddot{\nu}_0(t - t_0)^3 + ... \tag{3.3}$$

where N_0 is the pulse number at a reference time t_0.

However, our observing frame is not inertial since we are using telescopes located on a rotating Earth traveling in space. The center of mass of the solar system (barycenter), to a good approximation, is an inertial frame and corrections have to be applied to the measured topocentric TOAs before we can use them in equation 3.3 (Lorimer and Kramer, 2005).

$$t_{SSB} = t_{topo} + t_{corr} - t_{DM} + \Delta_{R_\odot} + \Delta_{S_\odot} + \Delta_{E_\odot} + \Delta_{R_B} + \Delta_{S_B} + \Delta_{E_B} \tag{3.4}$$

3.1.2 Clock and frequency corrections

The TOAs are usually determined by referring to the telescope local time (determined by the hydrogen maser at the GBT) but a more standard measure of time would be preferable. Therefore, the first correction in equation 3.4 (t_{corr}) can calculated by comparing the local time to the Coordinated Universal Time (UTC) obtained via the Global Positioning system (GPS). For higher precision timing (sub-μs), other time standards such as the Terrestrial Time (TT) should be used.

In the third term, the dispersion effect is removed from the data by referring the TOAs to the time that would be observed at an infinitely high frequency.

$$t_{DM} = \frac{DM}{2.41 \times 10^{-4} \times f^2} \tag{3.5}$$

This term is useful only when measurements are carried out at different observing frequencies. In this case, the resulting difference in dispersive delays between the sets of TOAs can be used to improve the DM value.

3.1.3 Solar system barycenter corrections

The *Roemer delay* ($\Delta_{R_\odot}$) is the first of 3 corrections necessary to transfer the TOAs from the topocenter to the solar system barycenter (SSB). Knowing accurately the positions of all major objects in the solar system, we can calculate the classical light-travel time from the SSB to the telescope. This requires an accurate ephemeris of the solar system such as the DE405 published by the Jet Propulsion Laboratory (Standish, 1998).

The next 2 terms are small general relativistic corrections to the barycenter. The *Shapiro delay* ($\Delta_{S_\odot}$) is caused by the curvature of space-time from the presence of masses in the solar system (Shapiro, 1964) and the *Einstein delay* ($\Delta_{E_\odot}$) represent the combined effect of time dilation and gravitational redshift caused by the bodies in the solar system (see Backer and Hellings, 1986, for an expression).

3.1.4 Binary pulsars corrections

The last 3 terms in equation 3.4 need to be incorporated in the timing model for pulsars in a binary system. They describe, respectively, the *Roemer, Shapiro and Einstein delay* and will transfer the TOAs to the center of mass of the binary system. Before we discuss the terms, a few words on the Keplerian orbital description is necessary.

The Keplerian description requires a minimum of five extra parameters in order to refer the TOAs to the barycenter of the binary system. They are the orbital period, P_b; the projected semi-major axis, $x = a_p \sin i / c$; the eccentricity, e; the longitude of periastron, ω; and epoch of periastron passage, T_0. These Keplerian parameters are all that is needed to describe the orbits in which relativistic effects can be ignored. In this case, the *Roemer delay* is given by (Blandford and Teukolsky, 1976)

$$\Delta_{R_B} = x(\cos E - e)\sin \omega + x \sin E \sqrt{1 - e^2} \cos \omega \tag{3.6}$$

where, in the non relativistic regime, the *eccentric anomaly, E*, is described in terms of the *mean anomaly, M* by Kepler's equation

$$E - e\sin E = M \equiv \frac{2\pi}{P_b}(t - T_0) \tag{3.7}$$

For binary pulsars with small eccentricity, the location of periastron is not well defined. To avoid the resulting correlation between ω and T_0, a different model is used (ELL1 in

TEMPO, Lange et al., 2001) where the epoch of ascending node; T_{ASC} and the first two Laplace-Lagrange parameters; ϵ_1 (e sin ω) and ϵ_2 (e cos ω) are used instead of e, ω and T_0.

Using only two of the classical Keplerian parameters, the projected semi-major axis and the orbital period, it is possible to place constraints on the companion mass via what is known as the *mass function*

$$f(m_p, m_c) = \frac{(m_c \sin i)^3}{(m_p + m_c)^2} = \frac{1}{T_\odot} \frac{4\pi^2}{P_b^2} x^3 \tag{3.8}$$

where the constant $T_\odot = GM_\odot/c^3 \simeq 4.92549$ μs. We use this expression to calculate a lower limit on the companion mass (m_c) by assuming an inclination $i = 90°$ and a typical pulsar mass $m_p = 1.35$ M$_\odot$ (Thorsett and Chakrabarty, 1999).

For orbital systems where relativistic effects, due to the strong gravitational field of the objects and the high orbital velocities typical of close binaries, are no longer negligible, extra parameters must be included in the timing models. Using the description offered by those *post-Keplerian parameters* (PK) (Damour and Deruelle, 1985, 1986), the previously mentioned Roemer delay can be modified to account for relativistic effects on the orbit. The last 2 terms of equation 3.4, the *Einstein* and *Shapiro delay*, can also be defined.

All of the post-Keplerian parameters can be written as functions of the masses in the binary system and the Keplerian parameters for any given theory of gravity (e.g. Damour and Deruelle, 1986). The easiest PK parameter to measure, given a highly eccentric orbit, is the relativistic advance of periastron, $\dot{\omega}$. A measurement of $\dot{\omega}$ yields the total mass of the system ($m_p + m_c$) and if combined to any other post-Keplerian parameter, leads to the unambiguous determination of m_p, m_c and the inclination i. Finally, measurement of a 3rd (or more) PK parameter would provide a consistency check for the assumed theory of gravity.

3.2 Solving new pulsars

Before we can extract information from the timing of pulsars, we must obtain a *phase connected* solution for newly discovered pulsars. Such a solution implies that we account for every individual rotation of the pulsar within the time span covered by the TOAs. Ideally, the starting point is a set of TOAs that were obtained from observations closely spaced in time. As we gradually build a model, we can fold the pulsar on more observations and increase the number of TOAs which in turn allow us to refine the model. When the model is coherent in phase, the difference between the observed and computed pulse phases, the residuals, is characterized by a gaussian distribution around zero with an RMS value that is comparable to the TOAs uncertainties. If the pulsar is isolated, the exercise is straightforward since there are not many parameters to fit for. We usually start by fitting for the pulse period and the reference phase and as we add more days, we have to include parameters like the frequency derivative and position.

Where things get more complicated is for binary pulsars. In that case, in order to start fitting for the binary parameters, we must have a pretty good initial guess at the orbit. There are a few tricks to do that and I will describe one that makes use of a program called FITORBIT from the Jodrell Bank Observatory. If the orbital period of a binary system is comparable to the length of the observation, it is possible to constrain the orbital parameters using the data from this single observation. However when the orbital period is significantly longer than any of the observations, detection of the pulsar on several closely spaced observations is necessary in order to determine the orbit. The first step involves finding good solutions for as many individual days as possible. Depending on the orbital

acceleration, several frequency derivatives may be necessary to obtain a good solution for a single day.

These solutions are then used to generate pulsar ephemerides that are expressed in terms of series of spin periods at different epochs. The ephemerides obtained from each day are then combined and FITORBIT is used to get a phase connected solution of the orbit. At this stage, if we do not have ephemerides for many closely spaced days, there is usually much degeneracy between the parameters and a good solution might be difficult to find. Hopefully, it will be good enough to fold the pulsar on a few extra days which will result in the expansion of the data set. Progress is made in an iterative manner until we judge the solution to be a good enough starting point. We can then use TEMPO to refine the parameters and then work our way toward a phase connected solution.

Chapter 4

Results

We have now searched and analyzed all of the early dense sets of observations in our globular cluster surveys as well as some of the subsequent timing observations. So far, we have discovered 23 new pulsars in 5 globular clusters, while some of the timing observations are still to be searched. All of the new pulsars have been discovered by me and a collaborator from NRAO, Scott Ransom. While the initial phase-connected timing solutions have been obtained from the collective effort of the members of our collaboration, I have obtained most of the final timing solutions reported here.

In this chapter, we will discuss the interesting properties of the new pulsars as well as derived constraints on the clusters themselves. The properties of the GCs used in this chapter are taken from various sources and summarized in Table 4.1. Since we do not have timing solutions for any of the new pulsars in NGC6522 and NGC6624, we will only report their basic discovery parameters. Even though I have searched extensively all of the dense early sets of observations of NGC6441, I have not found any of the new pulsars and will therefore also only report their parameters. The discussion will be limited to the globular clusters where we have phase connected timing solutions and I have made a significant contribution, namely M28 and NGC6440. Table 4.1 summarizes the basic parameters of M28 and NGC6440 that were used to interpret our results. No uncertainties could be found in the literature for the distances of the clusters as well as for the core velocity dispersion of NGC6440. In those cases, we used the values reported in Table 4.1 in our calculations. Because no measurement of the proper motion of NGC6440 could be found, it was assumed to be zero in our calculations.

The high dispersion measure (>100 cm^{-3} pc) of the new pulsars as well as the large observing bandwidth imply that they do not suffer from diffractive scintillation, resulting in the very high detection rate during the timing campaign. As a result, we now have phase connected coherent timing solutions with high precision spin, astrometric and binary information for most of the new pulsars. In all cases, the TOAs were fitted to a pulsar model containing spin and position parameters and binary parameters (where relevant) using TEMPO. The dispersion measure was fitted separately in two different ways. In most cases, the pulsars were detected in at least one of our two 820 MHz observations, providing a ~1000 MHz difference between the center frequency of both observations. However, for the pulsars that could not be detected at 820 MHz (M28G and M28E for example), TOAs were generated at different frequencies across the 600 MHz of bandwidth available at S-band. In both cases, frequency-dependent delays were used to obtain optimized values for the dispersion measure of each pulsar. In the case of M28A, the pulsar was strong enough to be seen at 820 MHz but significant changes in the profile shape (which has 3 components) between the two frequencies made the TOA generation using a unique standard profile too difficult a task and we decided to report the published value instead (Hobbs et al., 2004). Strong frequency evolution of the profile within our observing band made our subband DM slightly different from the published value.

The flux densities at 1400 MHz were first calculated at 1950 MHz using the radiometer equation to scale from the baseline rms, and then converted assuming a spectral index of -1.8 (Maron et al., 2000b). Because only one obervation was used to make the flux calculations

and they were not corrected for the position of the pulsars in the telescope beam, the reported values are highly uncertain and should be used only as guidelines.

For each pulsar, we report the position and rotational parameters and orbital elements (where relevant) from the timing measurements. For each binary pulsar, the orbit is described by the 5 Keplerian parameters presented in the previous chapter. For the small-eccentricity (or zero) binary pulsars, the epoch of ascending node (T_{ASC}) is measured instead of the epoch of periastron passage (T_0). The minimum companion mass is estimated assuming a pulsar mass of 1.35 $M_\odot$. In a few cases, we report the measurement of some post-Keplerian parameters as well.

The 3-level sampling of the Spigot introduces systematics on the profiles that are not well understood. Following standard pulsar timing practice in such cases, we compensate for this by increasing the uncertainties on the TOAs such that the reduced $\chi^2 \simeq 1$. All the uncertainties in the tables reporting the pulsar timing parameters (Tab. 4.2-4.3 and 4.8-4.9) are twice the fit uncertainties returned by TEMPO after the weighting of the errors and represent conservative estimates of 1 σ confidence levels.

M28

Parameter	Value	Reference
Center RA, α (J2000)	$18^h24^m32^s.9$	(Harris, 1996)
Center DEC, δ (J2000)	$-24°52'12''.0$	(Harris, 1996)
Distance, D (kpc)	5.6	(Harris, 1996)
Core radius (acrmin)	0.24 ± 0.06	(Trager et al., 1993)
Half-mass radius (acrmin)	1.6 ± 0.6	(Trager et al., 1993)
Central Surface Brightness (Vmags arcsec^{-2})	16.0 ± 0.2	(Trager et al., 1993)
Core velocity dispersion, $v_l(0)$ (km s^{-1})	8.23 ± 1.32	(Pryor and Meylan, 1993)
Proper motion in RA, μ_α (mas yr^{-1})	0.3 ± 0.5	(Cudworth and Hanson, 1993)
Proper motion in DEC, μ_δ (mas yr^{-1})	-3.4 ± 0.9	(Cudworth and Hanson, 1993)

NGC6440

Parameter	Value	Reference
Center RA, α (J2000)	$17^h48^m52^s.7$	(Harris, 1996)
Center DEC, δ (J2000)	$-20°21'37''.0$	(Harris, 1996)
Distance, D (kpc)	8.4	(Harris, 1996)
Core radius (acrmin)	0.13 ± 0.03	(Trager et al., 1993)
Half-mass radius (acrmin)	0.47 ± 0.08	(Trager et al., 1993)
Central Surface Brightness (Vmags arcsec^{-2})	17.0 ± 0.2	(Trager et al., 1993)
Core velocity dispersion, $v_l(0)$ (km s^{-1})	21.6	(Gnedin et al., 2002)

Table 4.1: Parameters of the 2 globular cluster M28 and NGC6440. The velocity dispersion in the core of NGC6440 was calculated from a model by Gnedin et al. (2002).

4.1 M28

M28 is a metal poor globular cluster at a distance of ∼5.6 kpc from the sun. Lyne et al. (1987) previously reported the discovery of a millisecond pulsar, the first of its kind in a globular cluster. During the course of this project, we have discovered 10 other millisecond pulsars in this cluster, 7 of which are in binary systems.

In Tab. 4.2, we report the position and rotational parameters of the 3 isolated pulsars in the cluster. The position, rotational parameters and orbital elements for the 2 binary pulsars with timing solutions are presented in Tab. 4.3 and 4.4.

The pulse profiles are presented in Fig. 4.1 for the isolated pulsars and in Fig. 4.2 for the binary pulsars.

The timing residuals for the isolated pulsars are presented in Fig. 4.3 as a function of time (MJD). For the binary pulsars, the residuals as a function of both time and phase are shown in Figs. 4.4 and 4.5.

For the 7 pulsars with a timing solution, their positions relative to the center of the cluster are presented in Tab. 4.5 and plotted in Fig. 4.6.

The DMs for the pulsars in M28 have an average value and standard deviation of (120.4 ± 1.4) pc cm^{-3}. The overall spread in DM, 4.5 pc cm^{-3}, is likely due to the large average DM as well as to irregularities in the ISM along the different lines of sight towards the pulsars. It is ∼6 times larger than what is observed for 47 Tuc and about half the value reported for Terzan 5. The only pulsar with an outlying DM, M28F, is located 15.4 core radii from the center of the cluster in the direction of the Galactic plane. Future proper motion measurements could confirm or refute its association with the cluster.

4.1.1 Individual pulsars

Eccentric binaries The pulsars M28C and M28D are both in highly eccentric orbits (e = 0.847 and 0.776 respectively) with companion masses of at least 0.26 M$_\odot$ and 0.38 M$_\odot$ respectively.

The use of early Parkes data coupled with the high eccentricity of M28C and its short orbital period has already enabled us to make a highly significant measure of the advance of periastron, $\dot\omega = (0.029816 \pm 0.000088)°\text{yr}^{-1}$. Assuming that the modification of the Keplerian orbit is due to general relativity, we can determine the total mass of the system to be $(1.616 \pm 0.014)\text{M}_\odot$. This information combined with the measured Keplerian mass function imply that the most likely (2σ) neutron star mass is $(1.31^{+0.04}_{-0.47})\text{M}_\odot$ (Fig. 4.7). GBT observations over the course of the next few years will likely yield a measurement of the varying delays caused by the gravitational redshift due to the presence of the companion and time dilation as the pulsar moves in its elliptical orbit. The two effects are summarized in the parameter γ. This parameter, along with the already precise measurement of $\dot\omega$, will provide a precise measurement of both masses, assuming that the companion's mass quadrupole is small and does not affect significantly the advance of periastron.

The longer orbital period of M28D and the greater uncertainties in the timing measurements have not permitted a significant measurement of the advance of periastron yet. More data are needed to achieve the level of certainty necessary to constrain the masses of both objects in the system. A surprising result is the relatively high period derivative $\dot P = (9.82 \pm 0.12) \times 10^{-17}$ s s^{-1} for a pulsar in a globular cluster. We are confident that this value is related to the slow down of the pulsar since it is at least 2 orders of magnitude greater than any other sources of acceleration which would altogether contribute to a maximum of ∼3% (see section 4.1.2). This implies either a mildly recycled or a young pulsar with a characteristic age of $\tau_c \sim 12.8$ Myr and a high surface magnetic field of B$_s \sim 8.96 \times 10^{10}$ G. M28D seems to lie in the gray zone between normal globular cluster millisecond pulsars (B$_s \leq 10^9$

G, P $\sim$ few ms) and the distinct group of high magnetic field, long period globular cluster pulsars (Lyne et al., 1996) which has very few members like PSR B1745-20A in NGC6440 (P = 288 ms, $\dot{P}$ = 4 × 10^{-16}; Lyne et al., 1996) and PSR B1820-30B in NGC6624 (P = 378 ms, $\dot{P}$ = 3.15 × 10^{-17}; Biggs et al., 1994). The presence of such a young pulsar in a very old stellar system like M28 ($\sim$14 Gyrs) is quite puzzling. It would be worth analysing X-ray observations to see if it shares properties with another young pulsar, the Vela pulsar.

The companions of both pulsars are not sufficiently massive to be neutron stars unless the inclination angles i of the systems are improbably low. In the case of M28C, if the companion was a main sequence star, we would not expect such a high eccentricity due to the orbital circularization (Tassoul, 1995) implying that the companion is probably a white dwarf. However, the regular pulsar recycling scenario results in a NS-WD binary in a nearly circular orbit from the tidal circularization during the mass-transfer. A scenario in which an isolated WD is exchanged for the low-mass WD that recycled the pulsar could result in the observed eccentricity. A more likely scenario for M28D is the off-center collision of the neutron star with a giant star. This could apply to M28C as well if, for example, the pulsar was recycled prior to the collision. Such an encounter would result in the disruption of the giant's envelope leaving its core in an eccentric orbit and creating a disk that could partially recycle the pulsar (Rasio and Shapiro, 1991; Ivanova et al., 2005).

Eclipsing pulsar The binary pulsar M28H is the only eclipsing binary that was found in the cluster. M28H has an orbital period of $\sim$10 hours and a projected semimajor axis of $\sim$0.31 R$_\odot$. The eclipse is total at 1400 MHz and was observed consistently between orbital phase $\sim$0.15 and $\sim$0.4 (Fig. 4.5). The minimum inferred companion mass is 0.17 M$_\odot$ and its Roche lobe radius $\sim$0.6 R$_\odot$. M28H would therefore be part of a class of eclipsing binaries with a mass function > 3×10^{-4} M$_\odot$ known as eclipsing low-mass binary pulsars (ELMBP) (Freire, 2005). Similar eclipsing pulsars with short orbital periods and 0.1-0.25 M$_\odot$ companions include M30A (P = 11.0 ms, P$_{orb}$ = 0.174 days; Ransom et al., 2004), PSR J0024-7204W in 47 Tuc (P = 2.35 ms, P$_{orb}$ = 0.133 days; Camilo et al., 2000) and PSR J1701-3006B in M62 (P = 3.59 ms, P$_{orb}$ = 0.145 days; Possenti et al., 2003).

Since the orbital separation of the system is $\sim$2.9 R$_\odot$ (for i $\simeq$60°), an eclipse duration of $\sim$25% of the orbital period corresponds to a physical size of the eclipsing region R$_E$ $\sim$2 R$_\odot$. As for the other eclipsing MSPs of this type, supposing an inclination of 90°, the sizes of plausible companion types is much smaller than R$_E$. In the case of a white dwarf, R$_{WD}$ $\sim$10^{-2} R$_\odot$ and for a main sequence companion, R$_{MS}$ $\sim$0.2 R$_\odot$. Even the Roche lobe radius is smaller than R$_E$ implying that most of the eclipsing material lies outside the companion's Roche lobe and has to be constantly replenished (e.g. Fruchter et al., 1990).

Eclipse delays of up to 2 ms are visible from Fig. 4.5 during eclipse ingress/egress. The presence of an additional electron column density in the eclipse region implied by this dispersive delay is calculated from N$_e$ $\sim$ 7.4 × 10^{17}$\Delta_{\mathrm{t,ms}}\nu_{\mathrm{GHz}}^2$ cm^{-2}, where the dispersive delay Δ_t is in ms and ν_{GHz} is the observing frequency (1.95 GHz). For M28H, this represents N$_e$ $\geq$ 5.6 × 10^{18} cm^{-2}, comparable to the value reported by Ransom et al. (2004) for M30A. Given the size of the eclipsing region mentioned previously, the additional electron density close to the eclipse boundary is therefore n$_e$ $\geq$ 4 × 10^7 cm^{-3} ($\sim$9 orders of magnitude greater than the ISM) and the corresponding plasma density ρ_e $\geq$ 7 × 10^{-17} g cm^{-3}.

M28H differs from the pulsars previously mentioned in one respect. In order to achieve the flat residuals shown in Fig. 4.5, a large orbital period derivative; $\dot{P}_{orb}$ = 2.46 (28) × 10^{-9} s s^{-1} was necessary, suggesting that the binary is losing material and is spiraling out to longer orbital periods (Czerny and King, 1988). In this respect it is more alike to PSR B1744-24A in Terzan 5 (P = 11.6 ms, P$_{orb}$ = 0.076 days, m$_c$ $\geq$ 0.087 M$_\odot$; Lyne et al., 1990)

We do not have solutions yet for the 2 binary pulsars M28I and M28K.

Isolated pulsars in M28

Parameter	J1824-2452A	J1824-2452B
α (J2000)	$18^h24^m32^s.00752$ (24)	$18^h24^m32^s.5456$ (19)
δ (J2000)	$-24°52'10''.497$ (62)	$-24°52'04''.29$ (50)
Dispersion measure (pc cm^{-3})	119.857	119.361 (18)
Pulsar period, P (ms)	3.0543154464578 (24)	6.546665363197 (12)
Period derivative, $\dot{P}$ ($10^{-15}s\ s^{-1}$)	0.00161917 (12)	-0.0002415 (94)
Epoch (MJD)	53,796.0	53,796.0
Span of timing data (MJD)	53,629-53,962	53,629-53,962
Number of TOAs	119	66
Weighted rms timing residual (μs)	1.33	34.21
Flux density at 1400 MHz, S_{1400} (mJy)	0.94	0.07

Parameter	J1824-2452E	J1824-2452F
α (J2000)	$18^h24^m33^s.08924$ (52)	$18^h24^m31^s.81284$ (22)
δ (J2000)	$-24°52'13''.57$ (18)	$-24°49'25''.029$ (48)
Dispersion measure (pc cm^{-3})	119.631 (19)	123.6079 (20)
Pulsar period, P (ms)	5.4191341975588 (36)	2.4511549181051 (11)
Period derivative, $\dot{P}$ ($10^{-15}s\ s^{-1}$)	-0.0001088 (26)	0.000009494 (24)
Epoch (MJD)	53,796.0	53,320.0
Span of timing data (MJD)	53,629-53,962	52,676-53,962
Number of TOAs	71	73
Weighted rms timing residual (μs)	12.84	6.09
Flux density at 1400 MHz, S_{1400} (mJy)	0.06	0.08

Table 4.2: The timing parameters for the isolated pulsars in M28. The dispersion measure of M28A is taken from Hobbs et al. (2004).
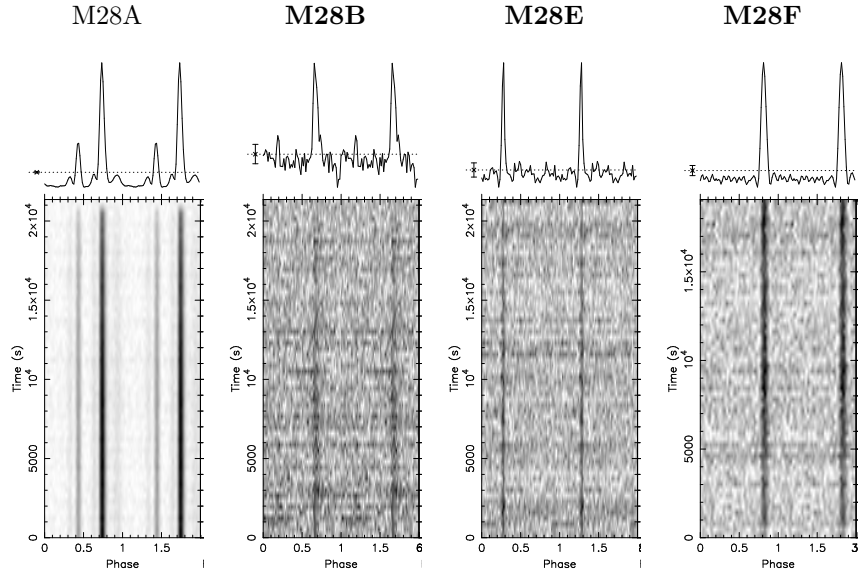

Figure 4.1: Integrated pulse profiles and grayscale plots as a function of time for the known pulsar M28A and the 3 isolated pulsars discovered in M28 (in bold). The timing parameters of all the isolated pulsars are listed in Tab. 4.2

Binary pulsars in M28

Parameter	J1824-2452G	J1824-2452H
α (J2000)	$18^h24^m33^s.02548$ (82)	$18^h24^m31^s.566$ (10)
δ (J2000)	$-24°52'17''.32$ (26)	$-24°52'06''.0$ (26)
Dispersion measure (pc cm^{-3})	119.674 (14)	121.532 (50)
Pulsar period, P (ms)	5.9090590374627 (56)	4.62941374446 (14)
Period derivative, $\dot{P}$ ($10^{-15}s\ s^{-1}$)	0.0001789 (40)	0.0000819 (62)
Epoch (MJD)	53,796.0	53,796.0
Span of timing data (MJD)	53,629-53,962	53,629-53,962
Number of TOAs	270	129
Weighted rms timing residual (μs)	33.17	33.69
Flux density at 1400 MHz, S_{1400} (mJy)	0.05	0.06
Binary Parameters		
Orbital period, P_{orb} (days)	0.1045836678 (72)	0.435027547 (28)
Projected semimajor axis, x (lt-s)	0.0164954 (58)	0.719450 (18)
Eccentricity, e	0.0	0.0
Epoch of ascending node, T_{ASC} (MJD)	53629.071809 (10)	53755.2263988 (13)
Longitude of periastron passage, ω (deg)	0.0	0.0
Post Keplerian Parameter		
Orbital period derivative, $\dot{P}_{orb}$ (10^{-9})		2.46 (28)
Derived Parameters		
Mass function, f_1 ($M_\odot$)	0.0000004406 (2)	0.00211277 (14)
Minimum companion mass, m_2 ($M_\odot$)	$\geq$0.0093	$\geq$0.17

Parameter	J1824-2452I	J1824-2452J
α (J2000)	$18^h24^m32^s.9$	$18^h24^m32^s.73362$ (58)
δ (J2000)	$-24°52'12''.0$	$-24°52'10''.18$ (32)
Dispersion measure (pc cm^{-3})	119	119.1408 (72)
Pulsar period, P (ms)	$\sim$3.9318	4.039689935267 (12)
Period derivative, $\dot{P}$ ($10^{-15}s\ s^{-1}$)	0.0	-0.0000757 (32)
Epoch (MJD)	53,758.0	53,750.0
Span of timing data (MJD)	53,738-53,781	53,629-53,962
Number of TOAs	32	395
Weighted rms timing residual (μs)		36.32
Flux density at 1400 MHz, S_{1400} (mJy)		0.07
Binary Parameters		
Orbital period, P_{orb} (days)	$\sim$0.459	0.0974313214 (38)
Projected semimajor axis, x (lt-s)	$\sim$0.768	0.0250221 (52)
Eccentricity, e	0.0	0.0
Epoch of ascending node, T_{ASC} (MJD)	$\sim$53758	53832.2815822 (36)
Longitude of periastron passage, ω (deg)	0.0	0.0
Derived Parameters		
Mass function, f_1 ($M_\odot$)		0.0000017720 (6)
Minimum companion mass, m_2 ($M_\odot$)		$\geq$0.015

Table 4.3: The timing parameters for the circular-orbit binary pulsars in M28. We do not have a good solution yet for M28I. The reported values are very uncertain and the parameters with no $\sim$ sign were not included in the fit. The dispersion measure reported for M28I is the best value found by prepfold and was fixed in the TEMPO fit.

Eccentric Binary pulsars in M28

Parameter	J1824-2452C	J1824-2452D
α (J2000)	$18^h24^m32^s.19212$ (10)	$18^h24^m32^s.422$ (18)
δ (J2000)	$-24°52'14''.658$ (24)	$-24°52'25''.9$ (7.4)
Dispersion measure (pc cm^{-3})	120.5698 (12)	119.87 (12)
Pulsar period, P (ms)	4.1582838256514 (16)	79.8354297394 (32)
Period derivative, $\dot{P}$ ($10^{-15}s\ s^{-1}$)	0.000170158 (12)	0.0982 (12)
Epoch (MJD)	53,320.0	53,796.0
Span of timing data (MJD)	52,676-53,962	53,629-53,962
Number of TOAs	910	108
Weighted rms timing residual (μs)	8.17	449.12
Flux density at 1400 MHz, S_{1400} (mJy)	0.17	0.05
Binary Parameters		
Orbital period, P_{orb} (days)	8.077806387 (26)	30.411507 (26)
Projected semimajor axis, x (lt-s)	7.357389 (12)	24.87142 (44)
Eccentricity, e	0.84704372 (82)	0.776334 (12)
Epoch of periastron passage, T_0 (MJD)	53756.59374573 (24)	53755.14835 (10)
Longitude of periastron passage, ω (deg)	137.604977 (56)	311.0920 (18)
Post Keplerian Parameter		
Advance of periastron, $\dot{\omega}$ (deg yr^{-1})	0.029816 (88)	
Derived Parameters		
Mass function, f_1 ($M_\odot$)	0.006553407 (34)	0.01786113 (98)
Minimum companion mass, m_2 ($M_\odot$)	$\geq$0.26	$\geq$0.38
Total mass, ($M_\odot$)	1.616 (14)	
Companion mass range, m_2 ($M_\odot$)	$0.29^{+0.47}_{-0.4}$	
Pulsar mass range, m_1 ($M_\odot$)	$1.31^{+0.04}_{-0.47}$	

Table 4.4: The timing parameters for the eccentric binary pulsars in M28. The uncertainties on mass ranges for the pulsar M28C and its companion are given at the 2σ level.
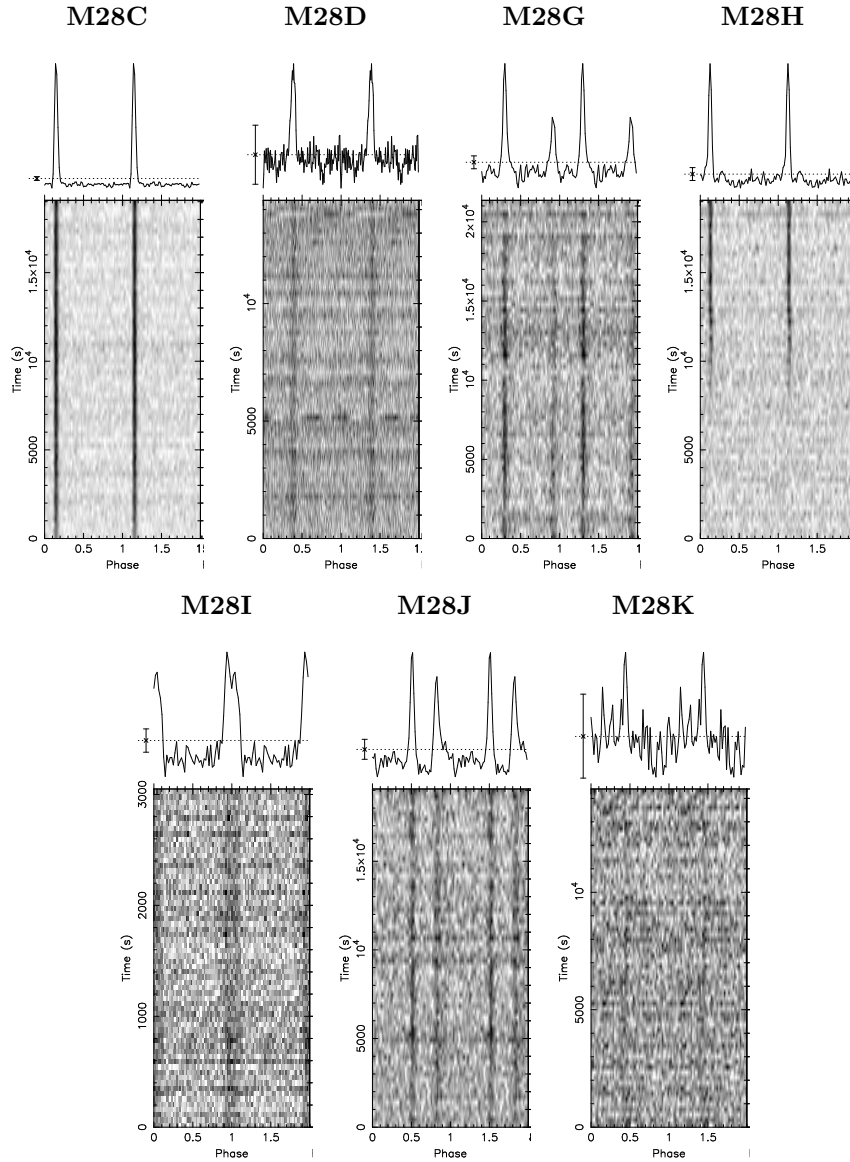
Figure 4.2: Integrated pulse profiles and grayscale plots as a function of time for the 7 binary pulsars discovered in M28. M28H is an eclipsing binary and can re-appear in mid-observation as shown in the plot. M28C and M28D are both highly eccentric binaries. The pulsar parameters are listed in Tab. 4.3 and 4.4.
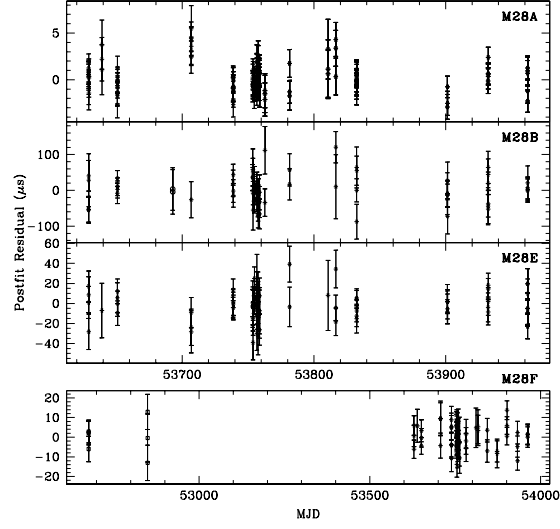
Figure 4.3: Timing residuals for the isolated M28 pulsars. M28F was detected in early Parkes data. We are confident that the large offset in the position of M28F from the center of the cluster is not the result of an error in the phase connection of the early Parkes data since it was measured first from our own observations.
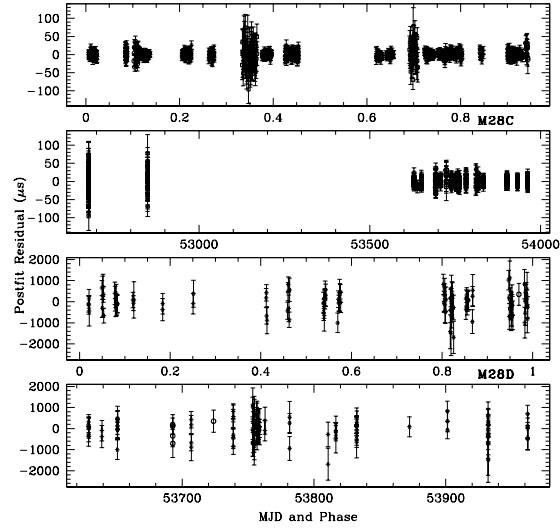
Figure 4.4: Timing residuals for the eccentric pulsars M28C (top 2 panels) and M28D (bottom 2 panels) as a function of time (MJD) and phase. Detection of M28C in early Parkes data helped increase the significance of our measured value for the advance of periastron $\dot{\omega}$.

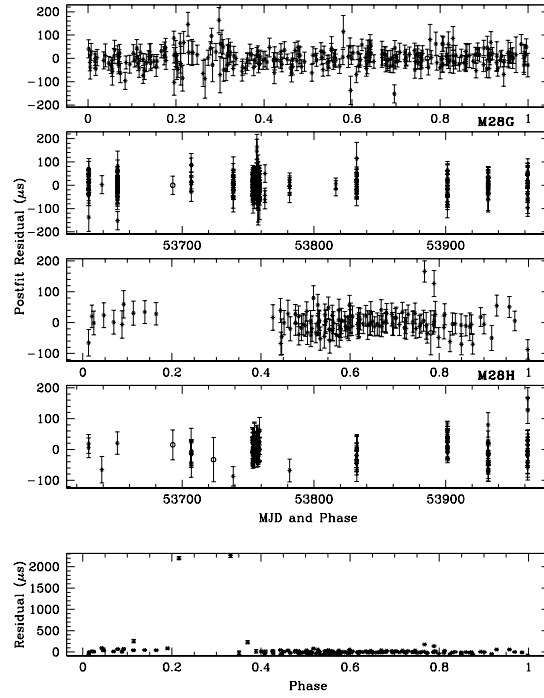Figure 4.5: Timing residuals for the binary pulsars M28G (top 2 panels) and M28H (bottom 2 panels) as a function of time (MJD) and phase. M28H is an eclipsing binary and the eclipse can clearly be seen from the lack of TOAs in the residuals between phase 0.15 and 0.40. The lower panel shows the same plot versus phase for M28H but with TOAs occurring during ingress/egress added. Eclipse delays of up to 2 ms are visible.

Pulsar offsets from the center of M28

Pulsar	x		y		$\theta_\perp$	
	(arcsec)	(core radii)	(arcsec)	(core radii)	(arcsec)	(core radii)
A	13.3872	0.930	1.503	0.104	12.2383	0.936
B	5.3160	0.369	7.71	0.535	9.09198	0.650
C	10.6182	0.737	-2.658	-0.185	9.99348	0.760
D	7.1700	0.498	-13.9	-0.965	15.3907	1.086
E	-2.8386	-0.197	-1.56	-0.108	3.01606	0.225
F	16.3074	1.133	166.97	11.60	167.625	11.65
G	-1.8822	-0.131	-5.32	-0.370	5.59363	0.392
H	19.9980	1.389	6.04	0.419	19.1209	1.451
J	2.4957	0.173	1.82	0.126	2.90623	0.214

Table 4.5: The positions of the M28 pulsars are given as east-west (x) and north-south (y) offset from the center of the cluster. The values are in arcsec and core radii ($r_c = 14.4$ acrsec). The last column is the projected radial distance from the pulsar to the cluster core. The center of the cluster is assumed to be exactly $\alpha = 18^h24^m32^s.9$ and $\delta = -24°52'12''.0$. (Harris, 1996)
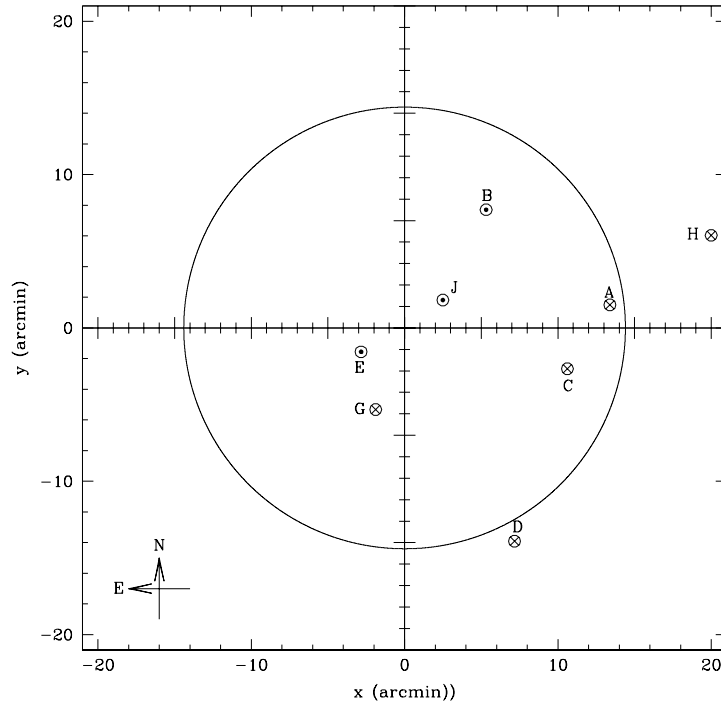
Figure 4.6: For the 9 pulsars with a timing solution in M28, the positions are plotted in the plane of the sky. The positions are plotted as east-west (x) and north-south (y) offsets from the center of the cluster (Tab. 4.5). The pulsars indicated with a $\otimes$ have a positive observed $\dot{P}$ and the pulsars with a $\odot$ have a negative $\dot{P}$. The core radius ($r_c = 14''.4$) is represented by a circle. The pulsar M28F is located 15.4 core radii from the core center and was omitted from the plot but its dispersion measure suggests that it is still associated with the cluster.

Figure 4.7: Plot of the companion mass as a function of the pulsar mass for the highly eccentric binary pulsar M28C assuming that $\dot{\omega}$ is purely due to general relativity. The hatched region is excluded by defi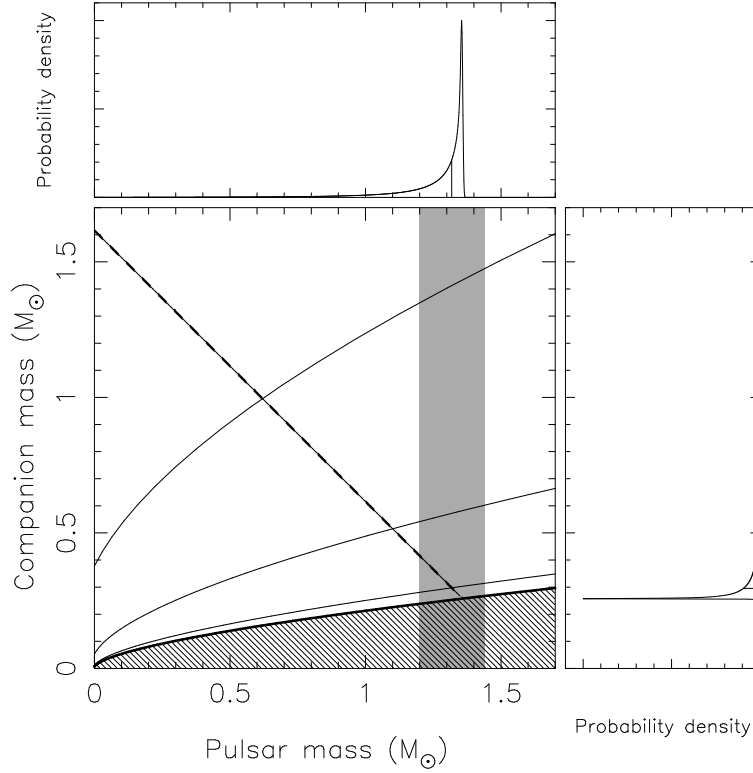nition of the Keplerian mass function ($\sin i \leq 1$). The diagonal line show the total system mass with 1-σ confidence intervals as measured by the general relativistic advance of periastron $\dot{\omega} = (0.029816 \pm 0.000088)^\circ\text{yr}^{-1}$. The probability density plots for both the companion (right plot) and pulsar (top plot) masses are calculated assuming a random distribution of inclination angles with a probability density flat in $\cos i$. The median values of the masses are indicated by vertical lines. The solid curves represent the constant inclinations (from bottom to top) of $i = 90^\circ$, 60°, 30° and 15°. The grey vertical line show the range of precisely measured NS masses from relativistic binary radio pulsars (Lattimer and Prakash, 2004). A 1-σ upper limit to the mass of the pulsar is 1.367 $M_\odot$.

4.1.2 Pulsar accelerations in the potential of M28

For three of the nine pulsars with timing solutions we report a negative period derivative (Tab. 4.2-4.3). However, this is not due to some intrinsic spin-up of the pulsar but more likely to the acceleration of the pulsar towards the Earth in the potential of the cluster. At least 4 components can contribute significantly to the acceleration of the pulsar along the line of sight (Phinney, 1993) and change the measured spin-down rate of a pulsar in a globular cluster. The observed period derivative $\dot{P}_{obs}$ is the sum of the intrinsic spin-down of the pulsar $\dot{P}_{int}$ and the acceleration components

$$\left(\frac{\dot{P}}{P}\right)_{obs} = \frac{a_G}{c} + \frac{a_{GC}}{c} + \frac{a_{PM}}{c} + \left(\frac{\dot{P}}{P}\right)_{int} \tag{4.1}$$

where a_G and a_{GC} are the line-of-sight components due to the acceleration caused by the gravitational potentials of the Galaxy and cluster respectively. The third component $a_{PM} = \mu^2 D$ is the apparent acceleration due to the transverse Doppler effect (Shklovskii, 1970) from the proper motion of the pulsar (which is taken to be the proper motion of the cluster) located at a distance D from the Earth. The acceleration components are reported in units of a/c (s^{-1}) such that they can be compared with the pulsars $\dot{P}/P$.

For M28, using the values in Table 4.1, we can estimate $a_G/c \simeq 1.1 \times 10^{-18}$ s^{-1} by assuming a spherically symmetric Galaxy with a flat rotation curve (Phinney, 1993) and $a_{PM}/c \simeq 1.6 \times 10^{-19}$ s^{-1}. Phinney (1993) showed that the globular cluster term, to an accuracy of 10%, is given by

$$max\frac{\mid a_{GC}\mid}{c} \simeq \frac{1.1G\bar{\Sigma}(<\Theta_\perp)}{c} \tag{4.2}$$

where $\bar{\Sigma}(<\Theta_\perp)$ is the projected surface mass density within the radial position of the pulsar $\Theta_\perp$.

Using optical measurements of the central surface brightness, we can calculate the projected surface luminosity density within the radius determined by the positions of the pulsars. It is then possible, using equation 4.2 to place a lower limit on the projected mass-to-light ratio within the radius of the pulsar's positions. These limits, presented in Table 4.6, are all typical for globular clusters.

Pulsar	$(\dot{P}/P)_{obs}$ $(10^{-17}$ s)	$R_\perp$ (pc)	$\bar{\Sigma}(<\Theta_\perp)$ $(10^3$ $M_\odot$ $pc^{-2})$	M / L $(M_\odot/L_\odot)$
B	-3.69	0.247	>75	>1.80
E	-2.01	0.082	>42	>1.01
J	-1.87	0.079	>39	>0.95

Table 4.6: Constraints on the projected surface mass density and mass-to-light ratio of M28 obtained from the pulsar with a negative $(\dot{P}/P)_{obs}$.

The maximum acceleration expected near the center of the globular cluster ($\Theta_\perp < 2\Theta_c$), within $\sim 10\%$, can be calculated with (Phinney, 1993)

$$max\frac{\mid a_{GC}(\Theta_\perp)\mid}{c} \simeq \frac{3}{2}\frac{v_l^2(\Theta_\perp)}{cD\sqrt{\Theta_c^2 + \Theta_\perp^2}} \tag{4.3}$$

where Θ_c is the core radius of the cluster and $v_l(\Theta_\perp)$ is the one-dimensional velocity dispersion (Tab. 4.1). Since we do not have an accurate function $v_l^2(\Theta_\perp)$, by using the value of the velocity dispersion for the cluster core $v_l(0)$ and making the conservative assumption

that the acceleration does not change with $\Theta_\perp$, we calculate the absolute upper limit on the acceleration $a_{GC}(0)/c$. If we account for the 1-σ error bars on the parameters in Table 4.1, the maximum possible value for the acceleration due to the cluster is calculated using D = 5.6 kpc, $v_z(0) = 9.55$ km s^{-1} and $\Theta_c = 0.236$ arcmin, leading to max $\frac{a_{GC}(0)}{c} = 3.847$ $\times 10^{-17}$ s^{-1}.

We can then calculate the maximum intrinsic period derivative for each pulsar and use them to obtain one-sided limits on their characteristic age and inferred surface dipole magnetic field strength. If we assume that each pulsar experiences the maximum acceleration, the upper limit on the intrinsic acceleration of the pulsars is given by

$$\left(\frac{\dot{P}}{P}\right)_{int} < max\frac{\mid a_{GC}\mid}{c} + \left(\frac{\dot{P}}{P}\right)_{obs} - \frac{a_G}{c} - \frac{a_{PM}}{c} \tag{4.4}$$

The resulting limits for the pulsar parameters obtained with this maximum constant acceleration are presented in Table 4.7. These limits were calculated independently of any modeling of the cluster, and are therefore extremely conservative.

Pulsar	P	$(\dot{P}/P)_{obs}$	$\dot{P}_{int}$	τ_c	B
	(ms)	(10^{-17} s)	(10^{-19})	(10^8 yr)	(10^9 G)
B	6.547	-3.69	<0.3	>37.7	<0.4
C	4.158	4.09	<3.4	>1.9	<1.2
D	79.835	123.11	~1020.	~0.12	~91.0
E	5.419	-2.01	<1.1	>7.5	<0.8
F	2.451	0.38	<1.1	>3.5	<0.5
G	5.909	3.03	<4.2	>2.2	<1.6
H	4.629	1.77	<2.7	>2.7	<1.1
J	4.040	-1.87	<0.9	>7.1	<0.6

Table 4.7: Upper limits on the period derivative, characteristic age and surface magnetic field for the M28 pulsars. The values were calculated with the cluster parameters from Tab. 4.1 in their lower limit; D = 5.6 kpc, $v_z(0) = 9.55$ km s^{-1} and $\Theta_c = 0.236$ arcmin. In this case, max$\frac{a_{GC}(0)}{c} = 3.847 \times 10^{-17}$ s^{-1}. Because the maximum contribution of all accelerations to the observed acceleration of M28D is of only ~3%, we believe that the calculated $\dot{P}_{int}$ is essentially accurate. In all other cases, the upper limits on $\dot{P}_{int}$ are close in magnitude to the expected intrinsic values for MSPs.

4.2   NGC6440

NGC6440 is a globular cluster at a distance of ∼8.4 kpc from the sun. In the initial target selection for our globular cluster pulsar search survey, it was ranked 4th due to the very high correlation between the number of X-ray point sources and the rate of stellar encounter in the cluster core (parametrized by Γ_c; Pooley et al., 2003). We believe that this parameter is a good indicator of the present rate of MSP formation. NGC6440 is also a well studied globular cluster in the X-ray and contains by far the largest number of low-mass X-ray binaries (LMXB) known in any cluster (Heinke et al., 2003). Lyne et al. (1996) had previously reported the discovery of a single slow millisecond pulsar, PSR B1745-20, with a spin period of 288 ms at a DM of 220 cm^{-3} pc. When compared to other millisecond pulsars, PSR B1745-20 has small characteristic age which seems to indicate ongoing pulsar formation in the cluster. NGC6440 has revealed many surprises with the discovery of 5 new pulsars with at least 3 in binary systems.

In Tab. 4.8, we report the position and rotational parameters of the 3 isolated pulsars in the cluster. The position, rotational parameters and orbital elements for the 2 binary pulsars with timing solutions are presented in Tab. 4.9.

The pulse profiles are presented in Fig. 4.8 for the isolated pulsars and in Fig. 4.9 for the binary pulsars.

The timing residuals for the isolated pulsars are presented in Fig. 4.10 as a function of time (MJD). For the binary pulsars, the residuals as a function of both time and phase are shown in Figs. 4.11, 4.12 (with accompanying profile showing the eclipse of NGC6440D in Fig. 4.13), and 4.14 and 4.15.

For the 5 pulsars with a timing solution, their position relative to the center of the cluster are presented in Tab. 4.10 and plotted in Fig. 4.16.

The DMs for the pulsars in NGC6440 have an average value and standard deviation of (223.3 ± 3.2) pc cm^{-1}, and an overall spread in DM of 7.8 pc cm^{-1}, comparable to what is observed for Terzan 5. The spread is still interpreted as being due to the large average DM as well as to irregularities in the ISM along the different lines of sight towards the pulsars.

4.2.1   Individual pulsars

Eccentric binaries   The pulsar NGC6440B is in a highly eccentric orbit with a companion of mass of at least ∼0.08 $M_\odot$. The high eccentricity of NGC6440B has already enabled us to make a significant measure of the advance of periastron, $\dot{\omega} = (0.00323 \pm 0.00080)°yr^{-1}$. Assuming that the modification of the Keplerian orbit is due to general relativity, we can determine the total mass of the system to be $(2.2 \pm 0.8)M_\odot$. The small mass function combined with this information (Fig. 4.17) implies that the most likely neutron star mass is either very large ∼2.0 $M_\odot$ or else, we would need an improbably low inclination angle ($\leq 7°$) in order to have a normal pulsar mass. A 3rd possibility is that the $\dot{\omega}$ is not entirely due to general relativity. If the pulsar raises tides on its companion, a nonzero mass quadrupole moment can contribute to the advance of periastron (Smarr and Blandford, 1976). A strong dependence on the radius of the companion implies that this contribution would be stronger in the case of a main sequence companion. In this case, an optical detection could be possible although the intrinsically low luminosity of such a low mass star and the extinction in the direction of the cluster would probably make the task too difficult. The value of $\dot{\omega}$ is still somewhat uncertain but continued timing of the pulsars in this cluster, will provide us with a better estimate of the total mass of the system in the months to come.

We do not have a phase connected timing solution for the pulsar NGC6440F but we do have a good enough estimate of its orbital parameters to discuss some of the interesting properties of the pulsar. It has a short orbital period P_{orb} ∼9.8 days and a minimum

companion mass of ~ 0.3 M$_\odot$. The companion is not sufficiently massive to be a neutron star unless the orbital inclination angle is almost face-on. If the companion was a main sequence star, we would expect to see eclipses for a number of inclinations. This option can not be ruled out at the moment because we lack good orbital coverage. The short measured spin period and the low companion mass suggest a NS-WD system where the neutron has been recycled through a period of stable accretion. In this scenario, tidal circularization usually results in extremely small intrinsic eccentricities, as is seen for the NS-WD systems in the Galactic disk. For NGC6440F, the measured eccentricity e $\sim$0.03 is too large to be produced by any primordial binary evolution channel, suggesting a significant perturbation during the close flyby of another object in the cluster (Heggie and Rasio, 1996).

Eclipsing pulsar The binary pulsar NGC6440D has an orbital period of $\sim$6.87 hours and projected semimajor axis of $\sim$0.4 light-second. It has been observed to eclipse on all observations covering the orbital phase $\sim$0.15 and $\sim$0.33. NGC6440D has a minimum companion mass of 0.12 M$_\odot$ and the corresponding eclipsing region has a physical size R$_E$ $\sim$1.2 R$_\odot$, somewhat bigger than the Roche lobe radius of the companion R$_L$ $\simeq$0.5 R$_\odot$. Similarities with M28H also suggest that the companion is either a WD or a main sequence star losing material through some wind, constantly replenishing the space outside its Roche lobe. The eclipse of NGC6440D is not always total (Fig. 4.13) suggesting a scenario in which the eclipse is caused by the grazing incidence of the pulsar beam on a wind of material from the companion. With such characteristics, NGC6440D would join M28H in the class of eclipsing low-mass binary mentioned before.

Eclipse delays of up to 1 ms are visible from Fig. 4.12 during eclipse ingress/egress. The implied additional electron column density in the eclipse region is calculated in the same manner as for M28H. For NGC6440D, this represents $N_e \geq 3 \times 10^{18}$ cm^{-2}. Given the size of the eclipsing region, the additional electron density close to the eclipse boundary is therefore $\geq 3 \times 10^7$ cm^{-3} and the corresponding plasma density $\rho_e \geq 5 \times 10^{-17}$ g cm^{-3}.

Pulsar planet? NGC6440C is, at least on first look, a very normal millisecond pulsar with a spin period of 6.23 ms. But the timing residuals show some very interesting systematics with time. As we can see in Fig. 4.14, the densely sampled epoch shows what might be a low-amplitude sinusoid with a period of $\sim$15-20 days. Interestingly, the rest of the data, although very sparsely sampled, also shows some ups and downs and those systematics were not present in the residuals of any of the 4 other pulsars with a timing solution in this cluster. We have carried out a Lomb-Scargle periodogram search (Lomb, 1976; Scargle, 1982) on the residuals to try and find periodicities (Fig. 4.18). In order to avoid problems with the periodogram search due to the clumping of the data in the original TOA file, we ran the search on a different set of TOAs where only one TOA was generated for each observation. This has revealed one period P = 21.63 days with a significant power (99.5% significance level) when the second strongest signal is barely above the 50% level. Fitting an orbit with a small semimajor axis and the orbital period found by the Lomb-Scargle search flattened the residuals (Fig. 4.15) and reduced the χ^2 from $\chi^2 = 483.84$ for 36 dof, to $\chi^2 = 209.81$ for 33 dof, corresponding to an F-test probability of 3.7×10^{-6} (i.e. the significance that the more complex model containing the three extra parameters for a circular Keplarian orbit is preferred is $1.0 - 3.7 \times 10^{-6} = 99.9996\%$). The TEMPO fit returned an orbital period P$_{\text{orb}}$ = (20.14 ± 0.78) days and a projected semimajor axis $x = (1.51 \pm 0.24) \times 10^{-5}$ light-second. The resulting mass function $\sim 9.10 \times 10^{-21}$ implies a minimum companion mass $\sim 6 \times 10^{23}$ kg, a Mars mass planet orbiting the pulsar at a distance $\sim$0.14 AU.

Moreover, there are clearly still some systematics in the data after fitting the orbit, indicating that one simple orbital model is not sufficient. A few possible explanations include the eccentricity of the orbit, free precession of the pulsar (although no significant

Isolated pulsars in NGC6440

Parameter	A	C
α (J2000)	$17^h48^m52^s.6869$ (50)	$17^h48^m51^s.17261$ (24)
δ (J2000)	$-20°21'37''.8$ (24)	$-20°21'53''.67$ (12)
Dispersion measure (pc cm^{-3})	219.27 (32)	227.084 (22)
Pulsar period, P (ms)	288.6027824375 (36)	6.2269327218802 (38)
Period derivative, $\dot{P}$ (10^{-15} s s^{-1})	0.39888 (60)	-0.00006015 (62)
Epoch (MJD)	53,731.0	53,730.0
Span of timing data (MJD)	53,478-53,983	53,478-53,981
Number of TOAs	197	320
Weighted rms timing residual (μs)	712.09	44.11
Flux density at 1400 MHz, S_{1400} (mJy)	0.39	0.07

Parameter	E
α (J2000)	$17^h48^m52^s.79930$ (44)
δ (J2000)	$-20°21'29''.51$ (22)
Dispersion measure (pc cm^{-3})	224.41 (10)
Pulsar period, P (ms)	16.264003403873 (22)
Period derivative, $\dot{P}$ (10^{-15} s s^{-1})	0.0003141 (36)
Epoch (MJD)	53,730.0
Span of timing data (MJD)	53,478-53,981
Number of TOAs	55
Weighted rms timing residual (μs)	32.16
Flux density at 1400 MHz, S_{1400} (mJy)	0.04

Table 4.8: The timing parameters for the isolated pulsars in NGC6440. All the observations were made with the GBT+SPIGOT at S-band. PSR J1748-2021A was previously known (Lyne et al., 1996).

variation in the profile shape was seen), timing noise or even the presence of multiple planets. At this stage, there are still many degeneracies and the data are too sparsely sampled to draw any conclusions about the system but a dense set of observations would enable us to investigate those possibilities. A proposal to this effect has been submitted to the GBT. Confirmation of the presence of this planet would have important implications for terrestrial planet formation and the possibility of life in globular clusters and elsewhere in the Galaxy.

Binary pulsars in NGC6440

Parameter	B	D
α (J2000)	$17^h 48^m 52^s.95241$ (32)	$17^h 48^m 51^s.64555$ (16)
δ (J2000)	$-20°21' 38''.98$ (12)	$-20°21' 07''.509$ (90)
Dispersion measure (pc cm^{-3})	220.862 (38)	224.907 (28)
Pulsar period, P (ms)	16.760127226929 (22)	13.4958203902466 (62)
Period derivative, $\dot{P}$ (10^{-15} s s^{-1})	-0.0003269 (16)	0.0005876 (10)
Epoch (MJD)	53,730.0	53,730.0
Span of timing data (MJD)	53,478-53,981	53,478-53,981
Number of TOAs	669	513
Weighted rms timing residual (μs)	56.98	41.32
Flux density at 1400 MHz, S_{1400} (mJy)	0.10	0.12
Binary Parameters		
Orbital period, P_{orb} (days)	20.5500046 (28)	0.2860686791 (12)
Projected semimajor axis, x (lt-s)	4.467017 (28)	0.3972016 (66)
Eccentricity, e	0.5701621 (68)	0.0
Epoch of periastron passage, T_0 (MJD)	53717.780211 (36)	53729.77049932 (62)
Longitude of periastron passage, ω (deg)	314.31665 (58)	0.0
Post Keplerian Parameter		
Advance of periastron, $\dot{\omega}$ (deg yr^{-1})	0.00323 (80)	
Derived Parameters		
Mass function, f_1 ($M_\odot$)	0.0002266271 (46)	0.000822196 (42)
Minimum companion mass, m_2 ($M_\odot$)	$\geq$0.08	$\geq$0.12
Total mass, ($M_\odot$)	2.20 (83)	
Companion mass range, m_2 ($M_\odot$)	$0.12^{+0.22}_{-0.03}$	
Pulsar mass range, m_1 ($M_\odot$)	$2.04^{+0.70}_{-0.67}$	

Parameter	F
α (J2000)	$17^h 48^m 52^s.7$
δ (J2000)	$-20°21' 37''.0$
Dispersion measure (pc cm^{-3})	220
Pulsar period, P (ms)	3.7936231 (12)
Period derivative, $\dot{P}$ (10^{-15} s s^{-1})	0
Epoch (MJD)	53,646.0
Span of timing data (MJD)	53,489-53,920
Number of TOAs	40
Weighted rms timing residual (μs)	185.48
Binary Parameters	
Orbital period, P_{orb} (days)	9.8294 (11)
Projected semimajor axis, x (lt-s)	9.5008 (55)
Eccentricity, e	0.0322 (43)
Epoch of periastron passage, T_0 (MJD)	53652.00 (12)
Longitude of periastron passage, ω (deg)	197.0 (43)
Derived Parameters	
Mass function, f_1 ($M_\odot$)	0.009530 (15)
Minimum companion mass, m_2 ($M_\odot$)	$\geq$0.3

Table 4.9: The timing parameters for the binary pulsars discovered in NGC6440 with the GBT+SPIGOT at S-band during this project. The values of m_2 have been calculated assuming a pulsar mass of 1.35 $M_\odot$. For NGC6440D, the epoch of ascending node is reported since the epoch of periastron passage is not well defined (e $\sim$0). Because we do not have a phase connected solution for NGC6440F, the reported errors are very conservative (10 times the fitted uncertainties from TEMPO). The parameters with no uncertainties were not fitted in the timing model.
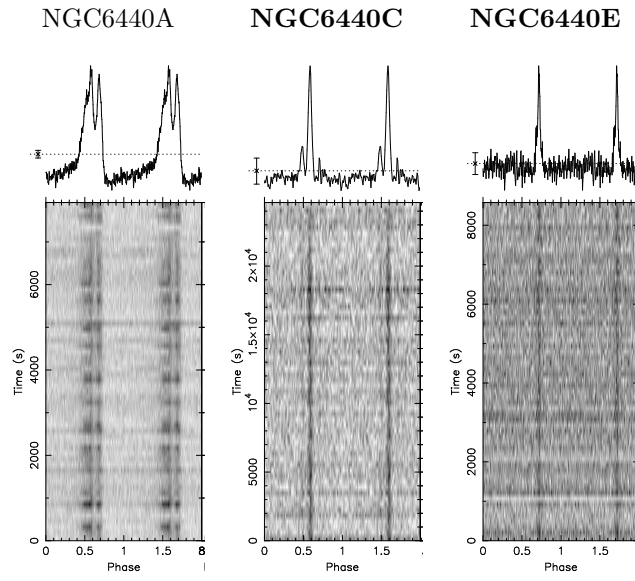
Figure 4.8: Integrated pulse profiles and grayscale plots as a function of time for the 2 isolated pulsars discovered in NGC6440 (in bold). The pulsar parameters are listed in Tab. 4.8
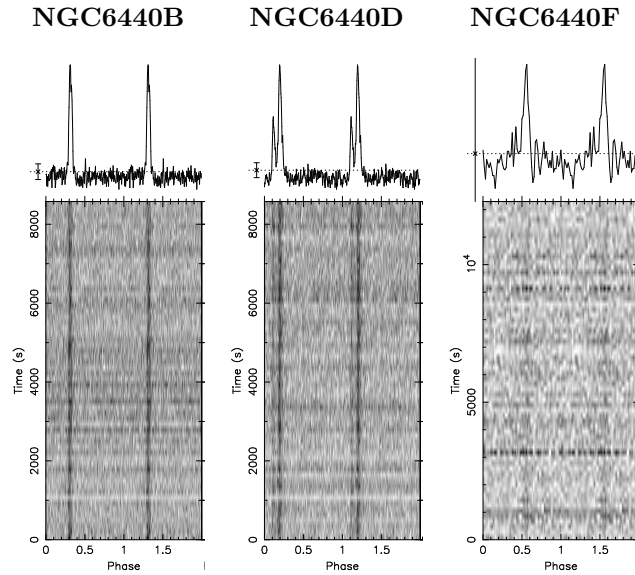

Figure 4.9: Integrated pulse profiles and grayscale plots as a function of time for the 3 binary pulsars discovered in NGC6440. The pulsar parameters are listed in Tab. 4.9
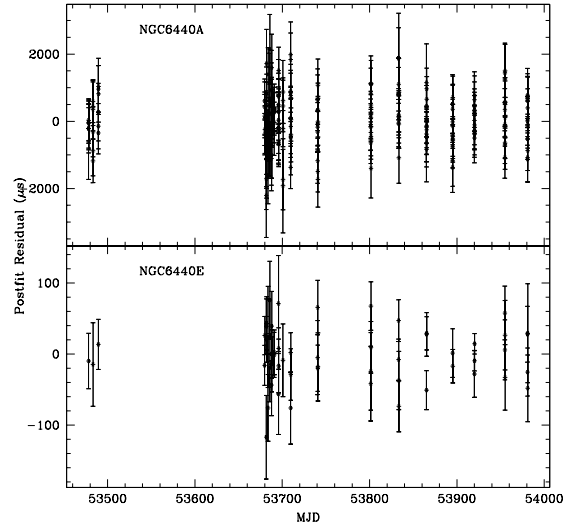
Figure 4.10: Timing residuals for 2 of the isolated NGC6440 pulsars as a function of time (MJD). The top panel shows the previously discovered NGC6440A and the bottom panel the new 16.26 ms pulsar NGC6440E.
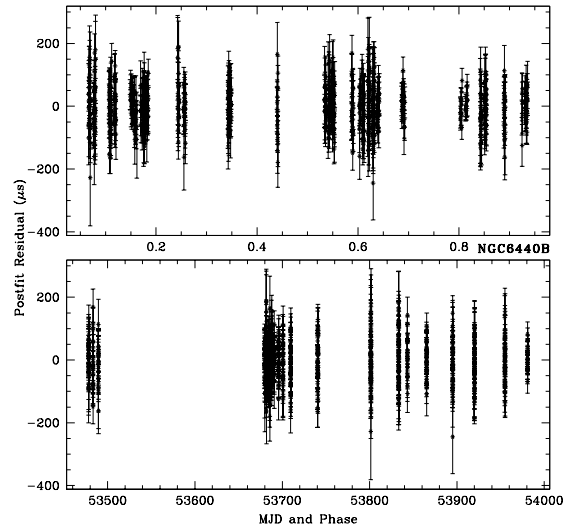

Figure 4.11: Timing residuals for the eccentric binary pulsar NGC6440B as a function of time (bottom panel) and phase (top panel).
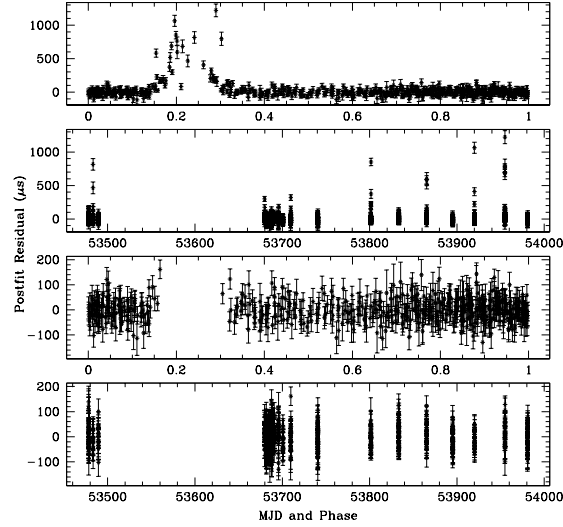
Figure 4.12: The bottom 2 panels show the timing residuals for the eclipsing binary pulsar NGC6440D as a function of time (MJD) and phase. All measured TOAs occurring between phase 0.15 and 0.32 were excluded from the fit in order to minimize systematic effects caused by pulse delays during the eclipse ingress/egress. Dispersive delays of about 1 ms from the extra electron content in the material causing the eclipse is evident from the top 2 panels where the TOAs occurring during the eclipse are shown. For a circular orbit, the eclipse is expected to occur during superior conjunction at phase 0.25.
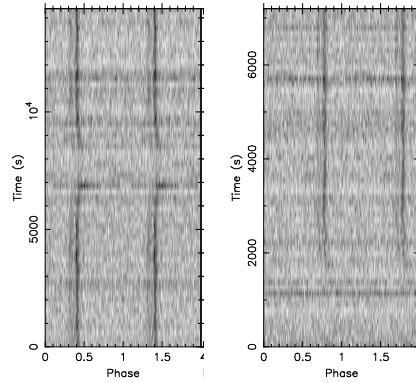

Figure 4.13: Grayscale plots of NGC6440D for 2 different observations where the pulsar shows the eclipse. On the left side, the eclipse is not total and the signal can be seem at all time while on the right side, the signal disappears completely for the duration of the eclipse. Also in the left panel, the dark horizontal signal at ∼7000 s is a good example of RFI.
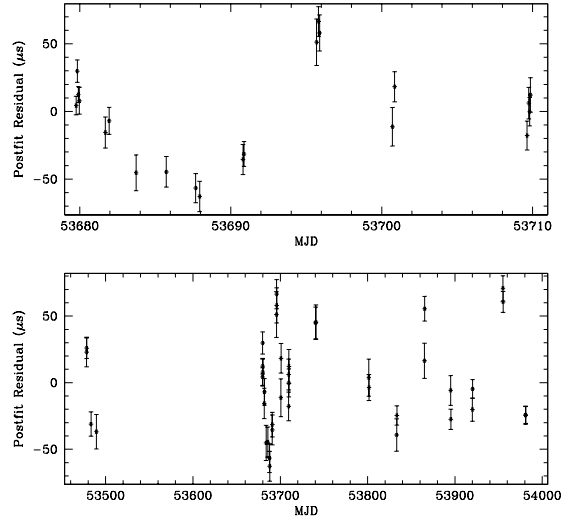
Figure 4.14: Timing residuals for pulsar NGC6440C. NGC6440C was first thought to be an isolated pulsar but some systematics in the residuals (bottom panel) suggest that a companion might be present. The top panel shows a zoom on the dense set of observations from January 2006 where a $\sim$20 days low amplitude sinusoid seems to be present.
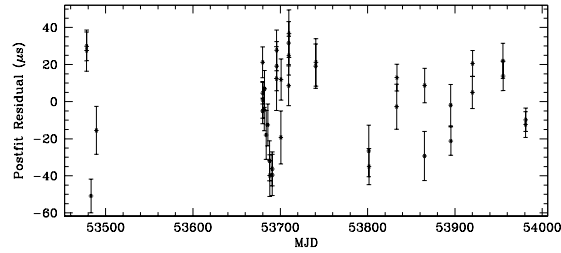

Figure 4.15: Performing a Lomb-Scargle periodogram search on the residuals (Fig. 4.18) revealed the presence of a significant periodicity (99.5% level). Fitting for orbital parameters resulted in a reduced χ^2 $\sim$50% lower and returned an orbital period $P_{orb} = (20.14 \pm 0.78)$ days and a projected semimajor axis $x = (1.51 \pm 0.24) \times 10^{-5}$ light-second. The mass functions suggest the presence of a Mars-mass companion orbiting the pulsar at a distance $\sim$0.14 AU. A fit using the second most significant periodicity did not improve the χ^2 as much. A dedicated timing campaign will be necessary to confirm our preliminary findings.

Pulsar offsets from the center of NGC6440

Pulsar	x		y		$\theta_\perp$	
	(arcsec)	(core radii)	(arcsec)	(core radii)	(arcsec)	(core radii)
A	0.1965	0.025	-0.822	-0.105	0.84	0.108
B	-3.786	-0.485	-1.983	-0.254	4.06	0.547
C	22.91	2.94	-16.67	-2.137	27.19	3.63
D	15.816	2.028	29.48	3.779	33.01	4.29
E	-1.488	-0.191	7.482	0.959	7.61	0.978

Table 4.10: The position of the M28 pulsars are given as east-west (x) and north-south (y) offsets from the center of the cluster. The values are in arcsec and core radii ($r_c = 7.8$ acrsec). The last column is the projected radial distance from the pulsar to the cluster core. The center of the cluster is assumed to be exactly $\alpha = 18^h24^m32^s.9$ and $\delta = -24°52'12''.0$.
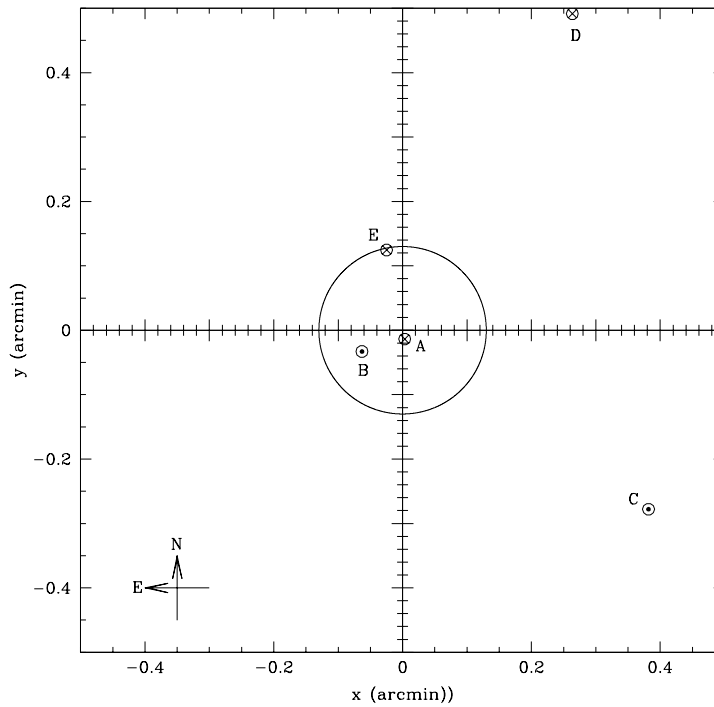

Figure 4.16: The position of the 5 pulsars with a timing solution in NGC6440 is plotted in the plane of the sky. The positions are plotted as east-west (x) and north-south (y) offsets from the center of the cluster (Tab. 4.10). The pulsars indicated with a $\otimes$ have a positive observed $\dot{P}$ and the pulsars with a $\odot$ have a negative $\dot{P}$. The core radius ($r_c = 0''.13$) is represented by a circle.
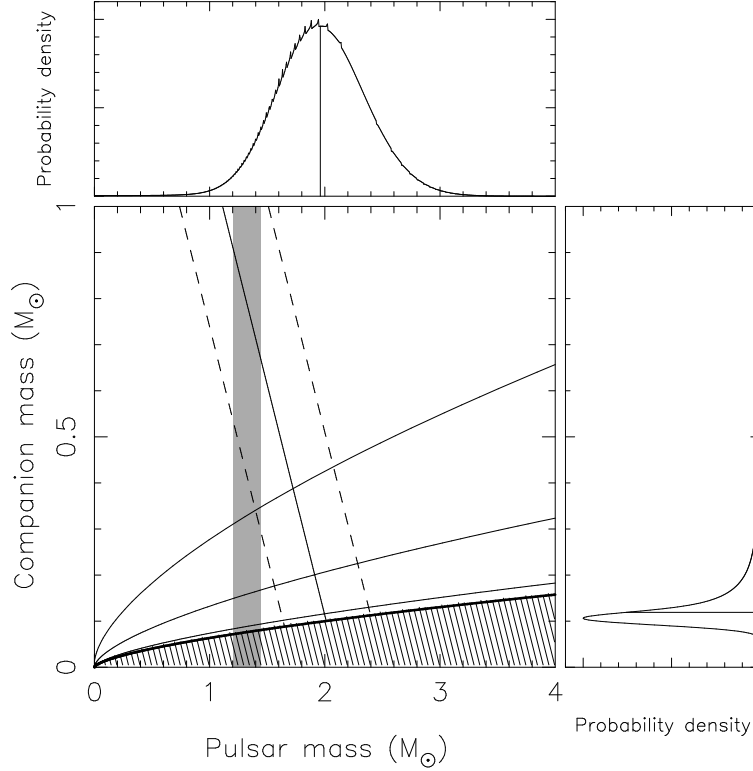
Figure 4.17: Plot of the companion mass as a function of the pulsar mass for the highly eccentric binary pulsar NGC6440B. The hatched region is excluded by definition of the Keplerian mass function (sin $i \leq 1$). The diagonal line shows the total system mass with 1-σ confidence interval from a measure of the advance of periastron $\dot{\omega} = (0.00323 \pm 0.00080)°\mathrm{yr}^{-1}$ supposing it is due to general relativity. The probability density plots (flat in cos i) for the pulsar (top plot) suggest an unusually high mass, well outside of the range of precisely measured NS masses (vertical gray band). Other explanations involves very low inclination angles or an $\dot{\omega}$ that is not entirely due to general relativity. The solid curves represent the constant inclinations (from bottom to top) of $i = 90°$, $60°$, $30°$ and $15°$.
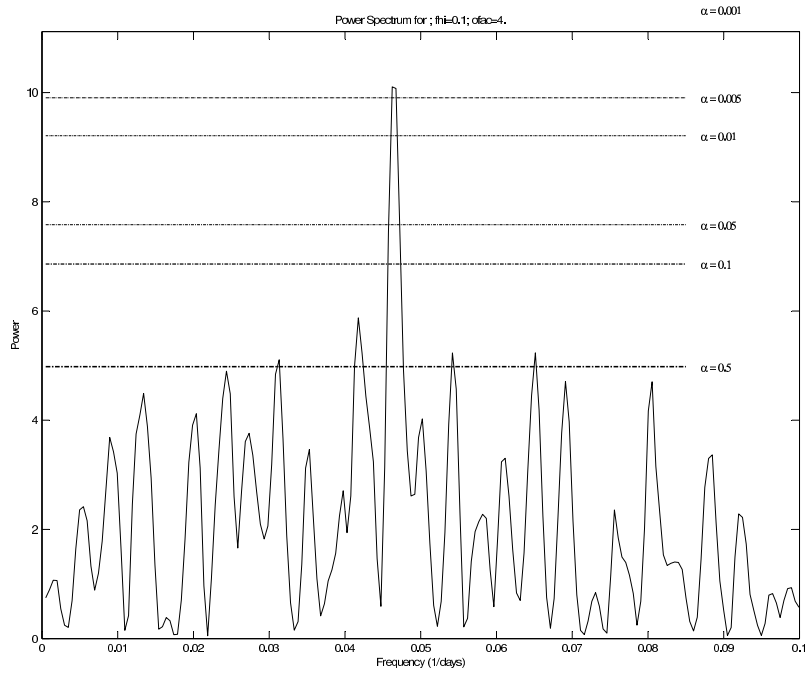
Figure 4.18: We performed a Lomb-Scargle periodogram search on the residuals of NGC6440C that revealed the presence of a periodicity (21.627 days) at the 99.5% significance level.

4.2.2 Pulsar accelerations in the potential of NGC6440

Applying the procedure discussed in 4.1.2 to NGC6440B, we can use the measured acceleration to place a lower limit to the projected mass-to-light ratio of the cluster within the radius of the pulsar position. In the case of NGC6440B, the measured acceleration is $(\dot{P}/P)_{obs} \simeq$ -1.95 × 10^{-17} s^{-1}. We can estimate the acceleration contribution from the Galaxy to be $a_G/c \simeq 2.3 \times 10^{-18}$ s^{-1}. The proper motion contribution can not be calculated from lack of the relevant information on the cluster.

Using equation 4.2, given the measured projected distance from the pulsar NGC6440B to the cluster core ($R_\perp \simeq 0.166$ pc), we calculate the minimum projected surface mass density $\bar{\Sigma}(< \Theta_\perp) \geq 34 \times 10^3$ M$_\odot$ pc^{-2} and the lower limit on the mass-to-light ratio M/L ≥ 0.284.

NGC6440C also has a negative measured $\dot{P}$ but was left out of the analysis because it is located too far from the cluster core.

The maximum acceleration expected near the center of the globular cluster can also be calculated from equation 4.3. Using D = 8.4 kpc, $v_z(0) = 21.6$ km s^{-1} and $\Theta_c = 0.18$ arcmin leads to max $\frac{a_{GC}(0)}{c} = 1.72 \times 10^{-16}$ s^{-1}. We can then calculate the maximum intrinsic period derivative for each pulsar and use them to obtain one-sided limits on their characteristic age and surface dipole magnetic field strength. The resulting limits are presented in Tab. 4.11. All these values are typical for millisecond pulsars.

Pulsar	P	$(\dot{P}/P)_{obs}$	$\dot{P}_{int}$	τ_c	B
	(ms)	(10^{-17} s)	(10^{-19})	(10^8 yr)	(10^9 G)
B	16.760	-1.95	<0.29	>0.92	<7.0
C	6.227	-0.96	<0.11	>0.87	<2.7
D	13.496	4.35	<0.32	>0.67	<6.6
E	16.264	1.93	<0.34	>0.75	<7.6

Table 4.11: Upper limits on the period derivative, characteristic age and surface magnetic field for the NGC6440 pulsars. The values were calculated with the values from Table 4.1 in their lower limits; D = 8.4 kpc, $v_z(0) = 21.6$ km s^{-1} and $\Theta_c = 0.18$ arcmin. In this case, $\frac{a_{GC}(R_\perp)}{c} = \frac{a_{GC}(0)}{c} = 1.72 \times 10^{-16}$ s^{-1}.

4.3   NGC6441

NGC6441 was chosen as a target in our survey because it has the $3^{\rm rd}$ largest rate of stellar encounters in its core (Γ_c) of all globular clusters in the Galaxy. Possenti et al. (2001) previously reported the discovery of a 111.6 ms binary pulsar in this cluster located at a distance of 11.7 kpc, establishing the dispersion mesure of the cluster to be about 233 cm^{-3} pc.

The phase-connected timing solutions for all 3 new pulsars in NGC6441 will soon be reported by other members of our collaboration. The basic parameters of the pulsars are reported in Tab. 4.12 and the profiles in Fig. 4.19.

New Pulsars in NGC6441

Pulsar	P_{psr} (ms)	DM (cm^{-3} pc)	Notes
NGC6441A	111.609	233	Known
NGC6441B	6.074	234	Isolated
NGC6441C	26.569	230	Isolated
NGC6441D	5.140	230	Eccentric Binary

Table 4.12: The new pulsars (in **bold**) discovered in NGC6441 with the GBT+SPIGOT at S-band during our survey. NGC6441B is a binary pulsar with an orbital period $P_{\rm orb} = 3.6$ days. The phase-connected timing solutions for all 3 new pulsars in NGC6441 will soon be reported by other members of our collaboration.
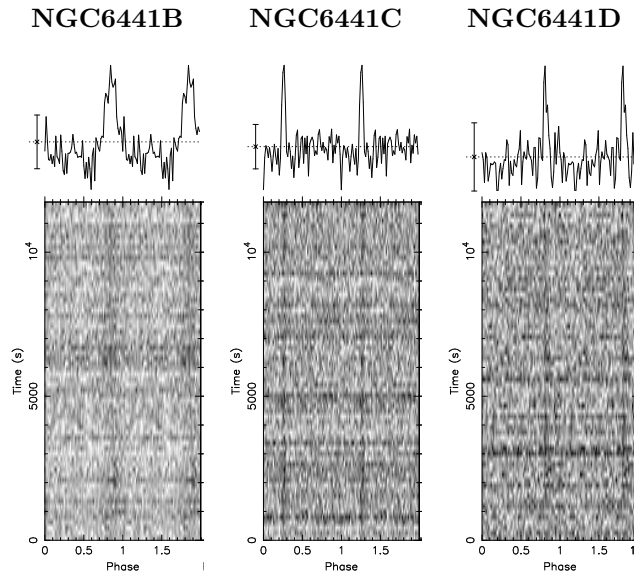

Figure 4.19: Integrated pulse profiles and grayscale plots as a function of time for the 3 pulsars discovered in NGC6441.

4.4 NGC6522

NGC6522 is a dense core collapsed cluster located at a distance of 7.8 kpc. Possenti et al. (2001) previously reported the discovery of a 7.101 ms isolated pulsar establishing the dispersion mesure of the cluster to be about 192 cm^{-3} pc.

On the 12th of September 2005, we observed the cluster for 4 hours. From this single observation, we found 2 millisecond pulsars by performing acceleration searches. The basic parameters of the pulsars are summarized in table 4.13 and the profiles in Fig. 4.20.

New Pulsars in NGC6522

Pulsar	P_{psr} (ms)	DM (cm^{-3} pc)	Notes
NGC6522A	7.101	192.0	Known
NGC6522B	4.397	192.6	Isolated
NGC6522C	5.840	194.5	Isolated

Table 4.13: The new pulsars (in **bold**) discovered in NGC6522 with the GBT+SPIGOT at S-band from a single observation conducted in September 2005. No timing campaign has been initiated yet.
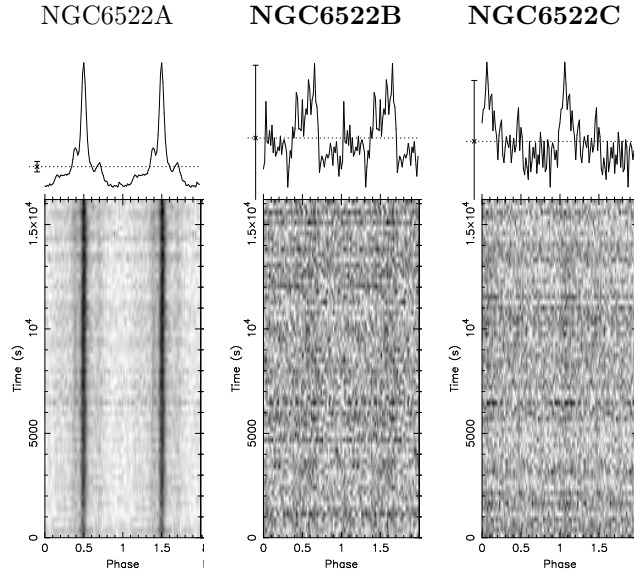

Figure 4.20: Integrated pulse profiles and grayscale plots as a function of time for the 3 pulsars in NGC6522 (new pulsars in **bold**). We do not know much about the pulsars at the moment (Tab. 4.13).

4.5   NGC6624

NGC6624 is a dense core collapsed cluster located at a distance of 7.9 kpc. Biggs et al. (1994) previously reported the discovery of 2 isolated pulsars: the 5.44 ms PSR B1820-30A and the slow 378.6 ms PSR B1820-30B. Chandler (2003) added to the collection another slow pulsar, the 405.9 ms J1824-2452C.

In September 2005, we observed the cluster for 4 hours. From this single observation, 3 millisecond pulsars were discovered, one of them by simple visual inspection of Fourier spectrum and the other two from acceleration searches. The basic parameters of the pulsars are summarized in table 4.14 and the profiles in Fig. 4.21. NGC6624F is very likely to be an eclipsing pulsar in a binary system but no conclusion can be drawn from this single detection.

<div align="center">

New Pulsars in NGC6624

Pulsar	P_{psr} (ms)	DM (cm^{-3} pc)	Notes
NGC6624A	5.440	86.8	Known
NGC6624B	378.596	87.0	Known
NGC6624C	405.9	87	Known
NGC6624D	3.020	86.9	Isolated
NGC6624E	4.394	91.4	Isolated
NGC6624F	4.850	86.7	Eclipsing

</div>

Table 4.14: The new pulsars (in **bold**) discovered in NGC6624 with the GBT+SPIGOT at S-band from a single observation conducted in September 2005. No timing campaign has been initiated yet.
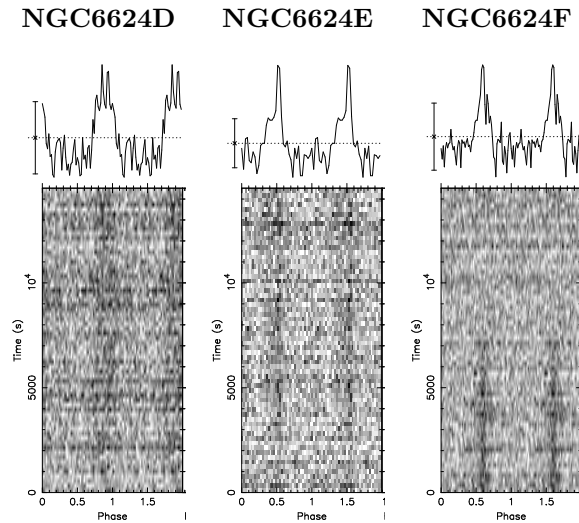

Figure 4.21: Integrated pulse profiles and grayscale plots as a function of time for the 3 new pulsars discovered in NGC6626. We do not know much about the pulsars at the moment (Tab. 4.14). The eclipse in NGC6624F is visible on the right plot.

4.6   Conclusions

With 23 new millisecond pulsars in 5 globular clusters, the results from the S-band survey I have taken part in represent a significant improvement in our knowledge, augmenting by ∼20% the total number of pulsars known in globular clusters.

One year of timing observations of the pulsars in M28 and NGC6440 has enabled us to find coherent timing solutions for 12 of the 15 new pulsars in those two clusters, 7 of which are in binaries.

Our discoveries include two rare eclipsing low-mass binary pulsars (M28H and NGC6440D). The existence of such systems is likely the result of exchange encounters and therefore should only be observed in globular clusters (Freire, 2005).

Also, for two (M28C and NGC6440B) of the three highly eccentric binaries, we have measured the relativistic periastron advance, yielding a measurement of the total system masses, assuming that $\dot{\omega}$ is purely due to general relativity. For M28C, we will be able to measure a 2nd post-Keplerian parameter in a few years and get a precise measurement of both masses. In the case of NGC6440B, we have found that either the most likely neutron star mass is above the range of well measured NS masses or the advance of periastron is not entirely due to general relativity but to a nonzero mass quadrupole moment from the companion. In this case, if the companion is a main sequence star, optical identification could, in principle, be done but might be precluded by the intrinsically low luminosity of such a low mass star and by the extinction in the direction of the cluster.

We have made a significant measurement of the intrinsic period derivative of M28D and found it unusually large for pulsar in a globular cluster. This suggest that it is either a mildly recycled pulsar, supporting a formation scenario involving the off-center collision of the neutron star with a giant star, or a surprisely young pulsar which should not be found in the very old stellar system like M28.

For some of the pulsars in M28 and NGC6440, we have used the negative period derivatives to place constraints on the mass-to-light ratio in the core of M28 and NGC6440 and found that they were typical of globular clusters.

We also derived limits for the ages and magnetic fields of the pulsars and found typical values for pulsars in globular clusters (except for M28D).

Finally, the greatest surprise comes from the potential presence of a Mars mass planet orbiting the pulsar NGC6440C with a period of ∼21 days at a distance of ∼0.16 Astronomical Units. We have submitted a proposal to the Green Bank telescope where we ask for a dedicated timing campaign that will enable us to confirm the presence of such an object.

Bibliography

Alpar, M. A., Cheng, A. F., Ruderman, M. A., and Shaham, J.: 1982, *Nature* **300**, 728

Baade, W. and Zwicky, F.: 1934, *Proc. Nat. Acad. Sci.* **20**, 254

Backer, D. C., Dexter, M. R., Zepka, A., D., N., Wertheimer, D. J., Ray, P. S., and Foster, R. S.: 1997, *PASP* **109**, 61

Backer, D. C. and Hellings, R. W.: 1986, *Ann. Rev. Astr. Ap.* **24**, 537

Backer, D. C., Kulkarni, S. R., Heiles, C., Davis, M. M., and Goss, W. M.: 1982, *Nature* **300**, 615

Bhattacharya, D. and van den Heuvel, E. P. J.: 1991, *Phys. Rep.* **203**, 1

Biggs, J. D., Bailes, M., Lyne, A. G., Goss, W. M., and Fruchter, A. S.: 1994, *MNRAS* **267**, 125

Binney, J. and Tremaine, S.: 1987, *Galactic dynamics*, Princeton, NJ, Princeton University Press, 1987, 747 p.

Bisnovatyi-Kogan, G. S. and Komberg, B. V.: 1974, *Sov. Astron.* **18**, 217

Blandford, R. and Teukolsky, S. A.: 1976, *ApJ* **205**, 580

Burgay, M., D'Amico, N., Possenti, A., Manchester, R. N., Lyne, A. G., Joshi, B. C., McLaughlin, M. A., Kramer, M., Sarkissian, J. M., Camilo, F., Kalogera, V., Kim, C., and Lorimer, D. R.: 2003, *Nature* **426**, 531

Camilo, F., Lorimer, D. R., Freire, P., Lyne, A. G., and Manchester, R. N.: 2000, *ApJ* **535**, 975

Camilo, F., Stairs, I. H., Lorimer, D. R., Backer, D. C., Ransom, S. M., Klein, B., Wielebinski, R., Kramer, M., McLaughlin, M. A., Arzoumanian, Z., and Müller, P.: 2002, *ApJ* **571**, L41

Chadwick, J.: 1932, *Nature* **129**, 312

Chandler, A. M.: 2003, *Ph.D. thesis*, California Institute of Technology

Clark, G. W.: 1975, *ApJ* **199**, L143

Cordes, J. M. and Lazio, T. J. W.: 2002, astro-ph/0207156

Cudworth, K. M. and Hanson, R. B.: 1993, *AJ* **105**, 168

Czerny, M. and King, A. R.: 1988, *MNRAS* **235**, 33P

D'Amico, N., Possenti, A., Fici, L., Manchester, R. N., Lyne, A. G., Camilo, F., and Sarkissian, J.: 2002, *ApJ* **570**, L89

Damour, T. and Deruelle, N.: 1985, *Ann. Inst. H. Poincaré (Physique Théorique)* **43**, 107

Damour, T. and Deruelle, N.: 1986, *Ann. Inst. H. Poincaré (Physique Théorique)* **44**, 263

Davies, M. B., Benz, W., and Hills, J. G.: 1992, *ApJ* **401**, 246

Davies, M. B. and Hansen, B. M. S.: 1998, *MNRAS* **301**, 15

Dewey, R. J., Taylor, J. H., Weisberg, J. M., and Stokes, G. H.: 1985, *ApJ* **294**, L25

Dicke, R. H.: 1946, *Rev. Sci. Instrum.* **17**, 268

Freire, P. C.: 2005, in Rasio and Stairs (2005), pp 405–417

Freire, P. C., Camilo, F., Kramer, M., Lorimer, D. R., Lyne, A. G., Manchester, R. N., and D'Amico, N.: 2003, *MNRAS* **340**, 1359

Freire, P. C., Camilo, F., Lorimer, D. R., Lyne, A. G., Manchester, R. N., and D'Amico, N.: 2001a, *MNRAS* **326**, 901

Freire, P. C., Kramer, M., and Lyne, A. G.: 2001b, *MNRAS* **322**, 885

Fruchter, A. S., Berman, G., Bower, G., Convery, M., Goss, W. M., Hankins, T. H., Klein, J. R., Nice, D. J., Ryba, M. F., Stinebring, D. R., Taylor, J. H., Thorsett, S. E., and Weisberg, J. M.: 1990, *ApJ* **351**, 642

Gnedin, O. Y., Zhao, H., Pringle, J. E., Fall, S. M., Livio, M., and Meylan, G.: 2002, *ApJ* **568**, L23

Goldreich, P. and Julian, W. H.: 1969, *ApJ* **157**, 869

Hankins, T. H. and Rickett, B. J.: 1975, in *Methods in Computational Physics Volume 14 — Radio Astronomy*, pp 55–129, Academic Press, New York

Harris, W. E.: 1996, *AJ* **112**, 1487, Updated version at http://www.physics.mcmaster.ca/resources/globular.html

Haslam, C. G. T., Stoffel, H., Salter, C. J., and Wilson, W. E.: 1982, *A&AS* **47**, 1

Heggie, D. C. and Rasio, F. A.: 1996, *MNRAS* **282**, 1064

Heinke, C. O., Grindlay, J. E., Lugger, P. M., Cohn, H. N., Edmonds, P. D., Lloyd, D. A., and Cool, A. M.: 2003, *ApJ* **598**, 501

Helfand, D. J., Manchester, R. N., and Taylor, J. H.: 1975, *ApJ* **198**, 661

Hessels, J. W. T., Ransom, S. M., Stairs, I. H., Freire, P. C. C., Kaspi, V. M., and Camilo, F.: 2006, *Science* **311**, 1901

Hewish, A., Bell, S. J., Pilkington, J. D. H., Scott, P. F., and Collins, R. A.: 1968, *Nature* **217**, 709

Hobbs, G., Lyne, A. G., Kramer, M., Martin, C. E., and Jordan, C.: 2004, *MNRAS* **353**, 1311

Hut, P., McMillan, S., Goodman, J., Mateo, M., Phinney, E. S., Pryor, C., Richer, H. B., Verbunt, F., and Weinberg, M.: 1992, *PASP* **104**, 981

Ivanova, N., Rasio, F. A., Lombardi, Jr., J. C., Dooley, K. L., and Proulx, Z. F.: 2005, *ApJ* **621**, L109

Jacoby, B. A., Cameron, P. B., Jenet, F. A., Anderson, S. B., Murty, R. N., and Kulkarni, S. R.: 2006, *ApJ*, In press, astro-ph/0605375

Johnston, H. M. and Kulkarni, S. R.: 1991, *ApJ* **368**, 504

Kaplan, D. L., Escoffier, R. P., Lacasse, R. J., O'Neil, K., Ford, J. M., Ransom, S. M., Anderson, S. B., Cordes, J. M., Lazio, T. J. W., and Kulkarni, S. R.: 2005, *PASP* **117**, 643

Kaspi, V. M. and Helfand, D. J.: 2002, in P. O. Slane and B. M. Gaensler (eds.), *Neutron Stars in Supernova Remnants*, p. 3, Astronomical Society of the Pacific, San Francisco

Kramer, M., Lyne, A. G., O'Brien, J. T., Jordan, C. A., and Lorimer, D. R.: 2006, *Science* **312**, 549

Krolik, J. H., Meiksin, A., and Joss, P. C.: 1984, *ApJ* **282**, 466

Landau, L. D.: 1938, *Nature* **141**, 333

Lange, C., Camilo, F., Wex, N., Kramer, M., Backer, D., Lyne, A., and Doroshenko, O.: 2001, *MNRAS* **326**, 274

Lattimer, J. H. and Prakash, M.: 2004, *Science* **304**, 536

Lattimer, J. M. and Prakash, M.: 2001, *ApJ* **550**, 426

Lomb, N. R.: 1976, *Astrophys. Space Sci.* **39**, 447

Lorimer, D. R. and Kramer, M.: 2005, *Handbook of Pulsar Astronomy*, Cambridge University Press

Lyne, A. G., Brinklow, A., Middleditch, J., Kulkarni, S. R., Backer, D. C., and Clifton, T. R.: 1987, *Nature* **328**, 399

Lyne, A. G., Burgay, M., Kramer, M., Possenti, A., Manchester, R. N., Camilo, F., McLaughlin, M. A., Lorimer, D. R., D'Amico, N., Joshi, B. C., Reynolds, J., and Freire, P. C. C.: 2004, *Science* **303**, 1153

Lyne, A. G., Johnston, S., Manchester, R. N., Staveley-Smith, L., D'Amico, N., Lim, J., Fruchter, A. S., and Goss, W. M.: 1990, *Millisecond pulsar in Terzan 5*

Lyne, A. G., Manchester, R. N., and D'Amico, N.: 1996, *ApJ* **460**, L41

Lyne, A. G. and Smith, F. G.: 1998, *Pulsar Astronomy, 2nd ed.*, Cambridge University Press, Cambridge

Manchester, R. N., Hobbs, G. B., Teoh, A., and Hobbs, M.: 2005, *AJ* **129**, 1993

Maron, O., Kijak, J., Kramer, M., and Wielebinski, R.: 2000a, *A&AS* **147**, 195

Maron, O., Kijak, J., Kramer, M., and Wielebinski, R.: 2000b, *A&AS* **147**, 195

Meylan, G. and Heggie, D.: 1997, *Astron. Astropys. Rev.* **8**, 1

Middleditch, J. and Kristian, J.: 1984, *ApJ* **279**, 157

Oppenheimer, J. R. and Volkoff, G.: 1939, *Phys. Rev.* **55**, 374

Padmanabhan, T.: 2001, *Theoretical Astrophysics, Volume 2: Stars and Stellar Systems*, Theoretical Astrophysics, by T. Padmanabhan, pp. 594. ISBN 0521562414. Cambridge, UK: Cambridge University Press, April 2001.

Phinney, E. S.: 1993, in S. G. Djorgovski and G. Meylan (eds.), *Structure and Dynamics of Globular Clusters*, pp 141–169, Astronomical Society of the Pacific Conference Series

Pooley, D., Lewin, W. H. G., Anderson, S. F., Baumgardt, H., Filippenko, A. V., Gaensler, B. M., Homer, L., Hut, P., Kaspi, V. M., Makino, J., Margon, B., McMillan, S., Portegies Zwart, S., van der Klis, M., and Verbunt, F.: 2003, *ApJ* **591**, L131

Possenti, A., D'Amico, N., Manchester, R. N., Camilo, F., Lyne, A. G., Sarkissian, J., and Corongiu, A.: 2003, *ApJ* **599**, 475

Possenti, A., D'Amico, N., Manchester, R. N., Sarkissian, J., Lyne, A. G., and Camilo, F.: 2001, Aspen Workshop: Compact Objects in Dense Star Clusters, astro-ph/0108343

Pryor, C. and Meylan, G.: 1993, in S. Djorgovski and G. Meylan (eds.), *ASP Conf. Ser. 50: Structure and Dynamics of Globular Clusters*, pp 357–371

Ransom, S., Hessels, J., Stairs, I., Kaspi, V., Freire, P., and Backer, D.: 2005, in Rasio and Stairs (2005), pp 199–205

Ransom, S. M.: 2000, in M. Kramer, N. Wex, and R. Wielebinski (eds.), *Pulsar Astronomy - 2000 and Beyond, IAU Colloquium 177*, pp 43–44, Astronomical Society of the Pacific, San Francisco

Ransom, S. M., Cordes, J. M., and Eikenberry, S. S.: 2003, *ApJ* **589**, 911

Ransom, S. M., Eikenberry, S. S., and Middleditch, J.: 2002, *AJ* **124**, 1788

Ransom, S. M., Hessels, J. W. T., Stairs, I. H., Freire, P. C. C., Camilo, F., Kaspi, V. M., and Kaplan, D. L.: 2005, *Science* **307**, 892

Ransom, S. M., Stairs, I. H., Backer, D. C., Greenhill, L. J., Bassa, C. G., Hessels, J. W. T., and Kaspi, V. M.: 2004, *ApJ* **604**, 328

Rappaport, S., Podsiadlowski, P., Joss, P. C., DiStefano, R., and Han, Z.: 1995, *MNRAS* **273**, 731

Rasio, F. and Stairs, I. H. (eds.): 2005, *Binary Radio Pulsars*, San Francisco, Astronomical Society of the Pacific

Rasio, F. A. and Shapiro, S. L.: 1991, *ApJ* **377**, 559

Scargle, J. D.: 1982, *ApJ* **263**, 835

Shapiro, I. I.: 1964, *Phys. Rev. Lett.* **13**, 789

Shapiro, S. L. and Teukolsky, S. A.: 1983, *Black Holes, White Dwarfs and Neutron Stars. The Physics of Compact Objects*, Wiley–Interscience, New York

Shklovskii, I. S.: 1970, *Sov. Astron.* **13**, 562

Sigurdsson, S.: 2003, in M. Bailes, D. J. Nice, and S. E. Thorsett (eds.), *ASP Conf. Ser. 302: Radio Pulsars*, pp 391–+

Smarr, L. L. and Blandford, R.: 1976, *ApJ* **207**, 574

Stairs, I. H.: 2003, *Living Reviews in Relativity* **6**, 5

Stairs, I. H.: 2004, *Science* **304**, 547

Standish, E. M.: 1998, *JPL Planetary and Lunar Ephemerides, DE405/LE405, Memo IOM 312.F-98-048*, JPL, Pasadena, http://ssd.jpl.nasa.gov/iau-comm4/de405iom/de405iom.pdf

Taam, R. E. and Sandquist, E. L.: 2000, *ARA&A* **38**, 113

Tassoul, J.-L.: 1995, *ApJ* **444**, 338

Taylor, J. H.: 1992, *Phil. Trans. Roy. Soc. A* **341**, 117

Taylor, J. H. and Huguenin, G. R.: 1969, *Nature* **221**, 816

Thorsett, S. E. and Chakrabarty, D.: 1999, *ApJ* **512**, 288

Trager, S., Djorgovski, S., and King, I.: 1993, in S. Djorgovski and G. Meylan (eds.), *Structure and dynamics of globular clusters*, Vol. 50, p. 347, ASp Conference series

Young, M. D., Manchester, R. N., and Johnston, S.: 1999, *Nature* **400**, 848